Escola de Camins
Escola Tècnica Superior d'Enginyeria de Camins, Canals i Ports
UPC BARCELONATECH

A multi-scale theoretical model for soft materials

TREBALL FINAL DE GRAU

Treball realitzat per:
Enric Martí Gallego

Dirigit per:
Pablo Sáez Viñas

Grau en:
Enginyeria Civil

Barcelona, 27 de setembre de 2018

Departament d'Enginyeria Civil i Ambiental

Contents

1 Introduction

Research in soft materials, from synthetic rubber to biological soft tissues, has been very active during the last century due to their importance in a wide range of technological applications, construction, cosmetic industry, automotive industry, plastics, adhesives etc. Today the relevance in the biological sector is increasing, appealing to the need to characterize accurately these materials. This characterization is carried out by studying their mechanical response, particularly, by analyzing mechanical tests of different materials. Soft materials include granular materials, colloidal suspensions, glasses, pastes, emulsions, foams, polymer networks, cells and many others. Their applicability in civil engineering and in the biological sector is on the rise because of their behavior. In the case of civil engineering, numerous studies where soft materials such as rubbers, elastomers and polymers are used with the aim of improving the properties of the structural elements. For instance, bitumen modified with waste tire rubber has been proved to affect to the fatigue performance of hot-mix asphalt(HMA), improving its fatigue resistance for medium traffic roads [2]. Analogous studies for the mechanical and durability properties of concrete with crumb rubber – coming also from waste tires – as a substitutive of fine aggregates has been also analyzed [3]. Another case of soft materials used in civil engineering would be in the bridge construction. Elastomeric bridge bearings connecting the deck with piers are able to undergo admissible rotations, vertical and horizontal forces. They can be composed of natural rubber or neoprene – can be steel-reinforced –, among others. As they require low cost and maintenance, elastomeric bridge bearings are commonly used in small and medium-sized bridges[4]. Moreover, elastomeric materials are usually used in expansion joints in bridges because its ability to absorb traffic loads and its temperature and fatigue resistance – See Figure 1.1 –.

In the biological sector, the study of mechanical properties of biological tissues is reaching more relevance. Most of the soft materials in the human body such as the brain, muscles, tendons, arteries, blood vessels and the skin are composed of macro-molecules(biopolymers). Studying their mechanical properties could useful in many areas, for instance, in injuries related to muscles or tendons, in modeling arteries and vessels, in the improve or replace of biological tissues (tissue engi-

Figure 1.1: Examples of civil engineering applications of soft materials. Elastomeric bridge bearing(left)[5] and expansion joint(right)[6].

neering), etc. And so, the analysis of the mechanical behavior of biological tissues can lead to understand better how tendons, muscles and the cardiovascular tissue work under mechanical loads. In Figure 1.2 two examples of biological tissues being stretched are presented.

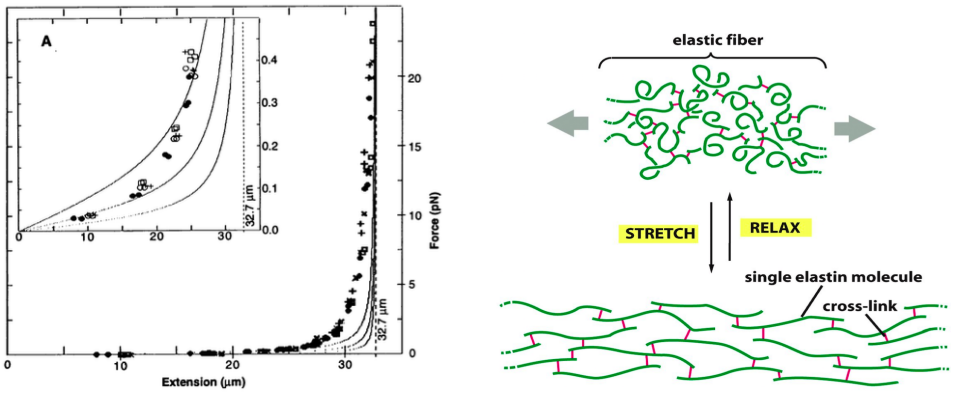

Figure 1.2: Examples of biological tissues under mechanical loads. DNA uniaxial tensile test(left figure)[1] and a schematic representation of a fiber of elastin being stretched(right figure)[7] .

1.1 Basic properties of Soft materials

Most of soft materials are composed of long chain molecules recognized as polymers. Thus, most of the models and physics underlying these materials are deduced from polymer physics. These polymeric chains are joined together by the so-called cross-linkers, which are commonly covalent bonds able to create complex network structures. There are also networks in which polymers are joined together by only physical entanglements, but this case will be not treated in the work. Furthermore, these networks are surrounded or even contained into a ground substance, usually contemplated as a liquid – for biological tissues would be water –, giving

to the whole structure of the material even more complexity. This complexity is related also to the fact that soft materials share several characteristics of the three states of matter: solid, liquid and gas[9]. Therefore, soft materials are able to exhibit elastic deformations with an almost full recovery – as conventional solid materials do –, but they can also be considered incompressible as a liquid may be. Additionally, attention will be paid in thermodynamic considerations – concerning to the relation with gas –, giving relevance to the entropy associated with the configurational changes in soft materials structure(presented in the following section).

Rubbers and biological tissues share several similarities – both can undergo non-linear elastic deformations, for example – , but some of their properties are accentuated in each group. Therefore, specifying separately these particularities or pronounced tendencies of each sub-group, may be useful to understand the models that will be applied to characterize their mechanical response.

1.1.1 Rubber-like materials

Thermoelastic properties of Rubber-like materials are particular because they contract under heating and expand upon cooling. By this fact can be also stated that rubber materials release heat when stretched. To most of rubber materials, not only can be attributed a great elasticity – reaching elongations up to 1000% [10] – but also their elasticity can be non-linear and sometimes followed by viscoelastic and time-dependent plastic effects [9].

Otherwise, not all rubbers or polymers are able to exhibit these properties. The temperature can play an important role. That is because there is a critical temperature different for each material, below from that, the material starts to approach a glasslike behavior(glassy state transition). Something similar would occur for what remains to crystallization. Some types of rubber can be crystallized or partially crystallized when being exposed to low temperatures for a prolonged time or even when getting stretched, leading these materials to not approach this elastic behavior just mentioned. This behavior is commonly accounted for the so-called vulcanized rubber, as a result of the process of vulcanization. Vulcanization is a chemical process able to create cross-links between individual chains in natural rubber or in polymeric chains [20]. This cross-linking prevents the network to move freely avoiding the tendency of plastic deformations and permitting to undergo an elastic deformation. This process is commonly done by heating the material with sulfur, suppressing the crystallization occurrence as well.

Although there are many types of rubbers each one with particular properties, in this work one is focusing in the non-linear elasticity that governs their mechanical behavior. This mechanical behavior can be related to the typical S-shaped stress-stretch curve of the uniaxial tension test. Figure 1.3 represents this typical behavior that will be treated in the applications of the models in following chapters. Rubber materials have been typically appealed to a macroscopic treatment, leaving in the background molecular structure considerations. The application of phenomenological models have been successfully applied, but in order to overcome

this lack of connection with the mechanical properties of the constituents, one will also apply Network models to reproduce the behavior of rubbers (See Chapter 2).

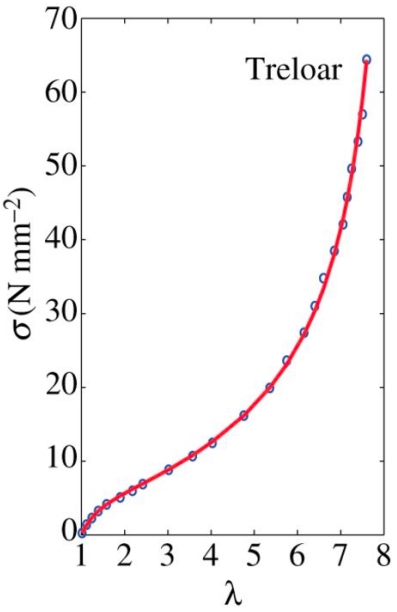

Figure 1.3: Representation of the typical non-linear *S-shaped* curve of an unaxial tension test in a rubber-like material [20].

1.1.2 Biological soft tissues

The connectives and cardiovascular tissues such as tendons, ligaments or arteries are constituted by the so-called extracellular matrices(ECMs). The ECMs are able to provide a physical structure in which cells are enclosed, forming a well-organized network of a mixture of cells and non-cellular components. They are also responsible of the regulation of some cellular processes such as growth, survival, migration etc.[12]. Although ECMs can be composed of a large and different constituents depending of the tissue, the principal components are proteins such as collagen, elastin and proteglycans(PGs)[11]. This work will be focused in the fibrous-forming networks of collagen and elastin.

Elastin is the major constituent of elastic fibers, and as its name may indicate, his principal biological function is to give elasticity to tissues[13]. Elastic fibers can be found mainly in blood vessels composing the cardiovascular system and in elastic ligaments among others. Alternatively, collagen is found in connective tissues such as tendons and cartilage, but is also found in skin, bones and arteries, being the most abundant protein in human bodies with about 25-30% [15]. Collagen is characterized through a fibrillar structure able to resist tensile, shear and compression forces, giving strength and providing the structural framework of tissues[14].

Apart from the biological function and mechanical behavior, the particularity of collagen and elastin is the structural configuration of their components. Their structures are characterized for a hierarchical organization of the forming chains. In collagen, the smallest scale is defined by molecules, then groups of molecules

are combined into fibrils, and analogously for fibers, fascicles and tendons — See Figure[1.2]–. This gives rise to one of the key challenge of these type of materials, which is how to relate and predict the local to the macroscopic strain, the degree to which micro-scale strains match the overall macro-scale network.

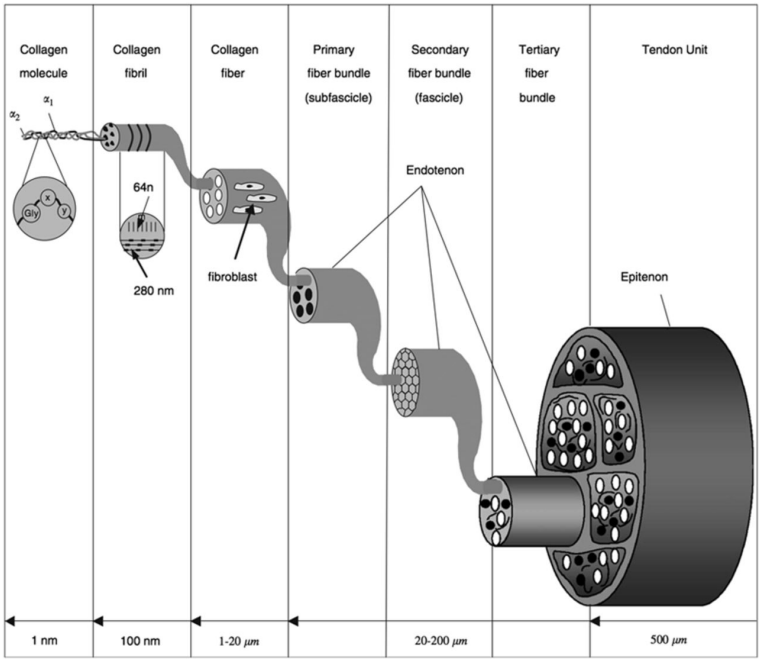

Figure 1.4: Hierarchical structure of collagen at different scales. The smallest scale corresponds to collagen molecules or tropocollagen reaching upper scales until to a tendon by the aggregation of their components [16].

These structural characteristics may be the reason for which soft materials are able to undergo not only large deformations but also a non-linear elastic response. This non-linearity comes, among others, from a phenomena often called strain-stiffening[17] for which is stated that biological tissues get stiffer as far as they approach larger strains. Strain stiffening may be caused because of the tendency of chains/fibers to reorient themselves into the stretch direction, making evidence that the preferential direction of chains influence to the behavior of the material. This leads to comment the importance of isotropy/anisotropy of soft materials, for which is accepted that the assumption of isotropy is sometimes found in the small strain regime[18]. The anisotropy of biological tissues is due to the disposition of their chains/fibers, they may be randomly distributed but it might be also a preferential direction. Orientation distribution functions (ODF) will be used to account for this dispersion.

1.2 Scope and Outline

The goal of this work is to explore a theoretical model for soft materials in general, starting by a review of the existing models that have been developed to describe

their mechanical behavior. Emphasis will be given to the relation between the mechanical response at the micro-scale and the macroscopic mechanical behavior of the network. Then, analyzing the mechanical behavior of the cardiovascular tissue and its main components – collagen and elastin – at different scales will be useful to understand this micro-macro transition.

The work is organized as follows: in Chapter 2 the models that describe soft materials' mechanical behavior are presented, separating them in two different approaches, one for the molecular or micro-level approach and other for a macroscopic treatment of soft materials. In the micro-level, the FLC and the WJC, the most common single-chain models, are explained. In the transition to the macroscopic scale, phenomenological and classical network models are reviewed in order to open the way to the full-network models.

In Chapter 3, these models are applied to experimental data. Following a least-square scheme, the characteristic material parameters are obtained from different materials. At the micro-scale, DNA and collagen molecules are treated. A macroscopic treatment of collagen and elastin fibrils is also done. Then, in the macroscopic scale, an example of rubber material is also tested with the classical network models. Finally, with the micro-sphere based model, the cardiovascular tissue is analyzed for all its network composed of collagen and elastin fibers.

Finally, in Chapter 4, the discussion of the results and conclusions of the work are exposed.

2 Models

2.1 Micro-mechanically based models

2.1.1 Entropic-based elasticity

As the chain-network is deformed, the orientation and distribution of these chains change, tending to a more organized disposition than the undeformed or initial configuration. As the thermoelasticity plays an important role in soft materials behavior, micro-mechanically based properties will be derived from the thermodynamic laws.

For an increase dl in length and being dU, dW and dQ the changes in internal energy, mechanical work and heat, respectively, the first law of thermodynamics constitutes that:

$$dU = dQ + dW \tag{2.1}$$

And getting the assumption that for soft materials, the internal energy at constant temperature is null ($dU = 0$)[20], the equation above remains:

$$dQ = -dW \tag{2.2}$$

As far as there is an increase in the length dl we can conclude that the mechanical work dW must be positive, which by Eq.[2.1] implies that dQ is negative(heat is given out on extension). Therefore, the heat that is released by the stretched material, is going to be equal to the work of the external forces expressed as:

$$dW = -TdS \tag{2.3}$$

So, changes of energy are related to the increment of entropy, and, as far as the deformed state has less entropy associated that the initial configuration, the energy that is needed to deform the material will be positive. That will be the reason why is accepted that a considerable contribution to the great elasticity of these materials is due to these changes of configurations just commented, leading to the

so-called entropic-elasticity[9]. The entropy associated to configurational changes will be expressed in terms of the probability p of having a certain configuration:

$$S = k_B \ln p \tag{2.4}$$

being $k_B = 1.3810^{-23} JK^{-1}$ the Boltzmann constant.

In terms of statistical mechanics, the entropy S is related to the number of microscopic configurations that, for a thermodynamic system in equilibrium, are compatible which its macro-state also considered in equilibrium [8]. It is also related to the grade of organization of the system. Then, to deal with micro-mechanically based models, a statistical treatment of the problem shall be done.

2.1.2 Single-chain models

Polymer chains have many conformations of nearly equal energy [18], and when stretched, the equilibrium state is altered creating entropic forces opposing those perturbations. As there is a large number of different configurations that a single chain may present, long chain molecules are commonly described in terms of statistical mechanics.

In the micro-mechanically based models the starting point is the definition of a representative single long chain molecule to then consider an assembly of many chains corresponding to the network. From all the micro-mechanically based models, we are focusing into the *Freely Jointed Chain model* and the *Worm-like Chain model*. As these models have a deep theoretical background, the main aspects are going to be presented, leaving apart tougher mathematical treatments.

Freely jointed chain model

The freely jointed chain model(FJC) is one of the simplest models used to describe polymers. Traditionally has been used more for rubber materials, but can be also used in biological tissues, as is going to be treated afterwards.

In the freely jointed chain model, an isolated long chain molecule is considered. These long chains are divided into *monomers*(sub-element associated to a polymer chain), and the union between these monomers can be recalled as *bonds*. Then, the FJC assumes that a long chain molecule composed of N bonds, has a fixed distance l between these bonds and also, by neglecting the interactions between monomers, can be considered that these monomers are *freely-oriented*. This fact not only assumes that their orientation must be completely independent of the orientation and position of the neighborings, but also that all the directions are of equal probability [18].

In Figure 2.1 the main parameters describing a FJC can be seen. The variable r corresponds to the end-to-end distance, defined as the vector joining the first and the last bond. Also can be recalled as r_0 the end-to-end distance in the reference of undeformed configuration. But the characteristic parameter of this model is the contour length $L = Nl$, that will be representative of the maximum extensibility

of the chain. The relation $r_0^2 = Nl^2$ is also fulfilled due to *uncorrelated* nature of the FJC [18][19].

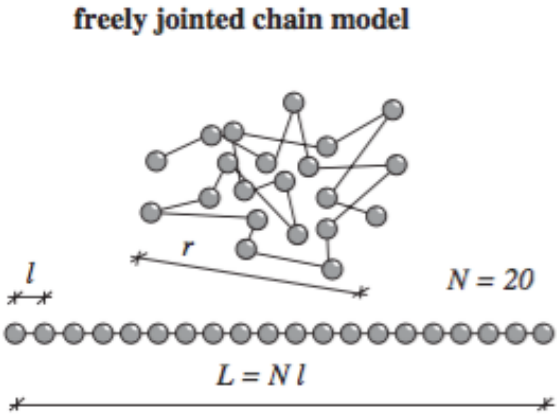

Figure 2.1: Schematic representation of the FJC, for N=20, taken from [18]

Before entering to the definition of the stress-stretch relation of FJC model, we first present the essential kinematic variables that will be useful for the FJC. The dimensionless ratio between the end-to-end distance r and the contour length is called the relative chain stretch λ_r while the chain stretch λ is defined by the quotient between the end-to-end distance r in the stretched configuration and the end-to-end distance r_0 in the undeformed state. All these conditions are expressed as follows:

$$\lambda = \frac{r}{r_0} \quad \text{with} \quad \lambda \in [1, \sqrt{N}) \tag{2.5}$$

$$\lambda_r = \frac{r}{L} = \frac{\lambda}{\sqrt{N}} \quad \text{with} \quad \lambda_r \in [N^{-\frac{1}{2}}, 1] \tag{2.6}$$

By these definitions, the FJC model is defined in terms of the free energy W associated to its configurational disposition as presented in Eqs. 2.3, 2.4. The configuration that a certain chain may take is commonly expressed in terms of the end-to-end distance r, and by the probability distribution that r could have, can be distinguished between the Gaussian FJC and the non-Gaussian FJC. Considering a Gaussian FJC with one end fixed in the origin of the Cartesian axes and the other in a point P of a three-dimensional space, the distribution of the probability $p(r_x, r_y, r_z)$ associated to this configuration will approach the gaussian probability function[20]:

$$p(r_x, r_y, r_z) = \left(\frac{3}{2r_0^2\pi}\right)^{\frac{3}{2}} e^{-\left(\frac{3}{2r_0^2}(r_x^2+r_y^2+r_z^2)\right)} \tag{2.7}$$

To more simplicity is going to be considered the one dimensional case by aligning the chain into the x-Axe. That will reduce Eq. 2.7 to:

$$p = \left(\frac{3}{2r_0^2\pi}\right)^{\frac{1}{2}} e^{\left(\frac{3r^2}{2r_0^2}\right)} = \left(\frac{3}{2r_0^2\pi}\right)^{\frac{1}{2}} e^{\left(\frac{3}{2}\lambda^2\right)} \tag{2.8}$$

By applying Eq. 2.4 the of entropy associated will be:

$$S = k_B \ln\left(p_0 e^{-\left(\frac{3}{2}\lambda^2\right)}\right) = k_B \ln p_0 - \frac{3}{2}\lambda k_B \tag{2.9}$$

being $p_0 = (\frac{3}{2r_0^2\pi})^{\frac{1}{2}}$. Getting this at hand and within Eq. 2.3 we obtain the free energy associated to the classical Gaussian treatment of the FJC:

$$W_{gau}^{fjc} = W_0^{fjc} + k_B T \frac{3}{2}\lambda^2 = W_0^{fjc} + k_B T \frac{3}{2}{\lambda_r}^2 \tag{2.10}$$

being $w_0^{fjc} = -k_B T \ln p_0$ the free energy in the unperturbed or unstrained state. To obtain the force [N] associated, it is only necessary to derive this expression respect to the end-to-end distance r:

$$f_{gau}^{fjc} = \frac{\partial W}{\partial r} = \frac{\partial W}{\partial \lambda} \cdot \frac{\partial \lambda}{\partial r} = \frac{3k_B T}{r_0}\lambda = \frac{3k_B T}{l}\lambda_r \tag{2.11}$$

giving a linear function depending on the stretch. The Gaussian statistic is used in many models due to its simplicity to describe the behavior of the material, but it also gives a general and not accurate description at high strain ranges. To give a more detailed characterization of the material behavior, specially in the large strain range, a non-Gaussian statistic is alternatively used. This alternative must be taken into account at deformations such that the end-to-end distance r begins to approach the contour length $L = Nl$(approximately when $r/L \simeq 0.4$, see Figure 2.2).

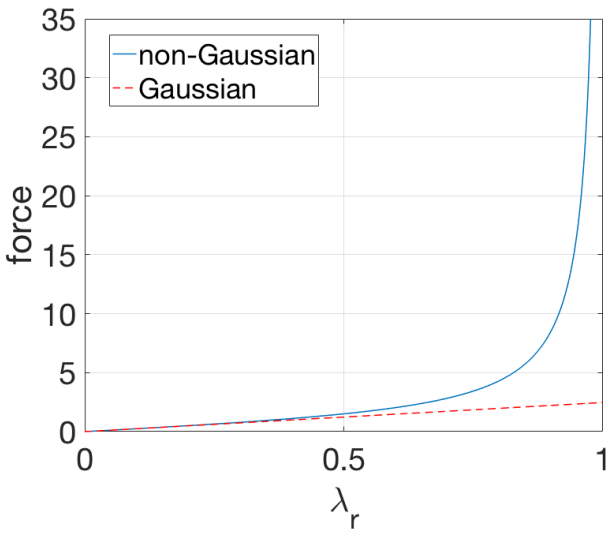

Figure 2.2: Comparison between Gaussian and non-Gaussian FJC. The solid line represents the non-Gaussian behavior of the FJC – by the inverse Langevin statistic –, while the dashed line describes the behavior for a Gaussian chain. Up to a range of $\lambda_r \simeq 0.4$ both statistics describe the same path, but then the non-Gaussian FJC approaches better the non-linearity of soft materials.

Therefore, the inverse Langevin function has been commonly used in order to describe the non-extensibility of the chain[9][18][20][22]. This function is usually defined in terms of the relative stretch λ_r and by the factor β as:

$$\frac{r}{L} = \lambda_r = \mathcal{L}(\beta) = \coth\beta - \frac{1}{\beta} \tag{2.12}$$

isolating β from this equation it will be obtained the operator inverse Langevin, expressed as:

$$\beta = \mathcal{L}^{-1}(\frac{r}{L}) \tag{2.13}$$

Afterwards, given the probability density $p(\lambda)$ expressed in terms of the inverse Langevin statistic, it can be obtained the strain energy function as it follows:

$$p(\lambda_r) = p_0 e^{\left(-\frac{Nr}{L}\beta - N\ln\left(\frac{\beta}{\sinh(\beta)}\right)\right)} \tag{2.14}$$

$$W_{lan} = W_0 + k_B T N \left[\lambda_r\beta + \ln\left(\frac{\beta}{\sinh(\beta)}\right)\right] \tag{2.15}$$

being k_B the Boltzmann constant, T the absolute temperature and N the number of bonds in the chain. To find the force-stretch relation, the strain energy function shall be derived with respect to the stretch, depending the variable to analyze. Again, the derivation with respect to r is presented considering $f = \frac{\partial W}{\partial r} = \frac{\partial W}{\partial \lambda_r} \cdot \frac{\partial \lambda_r}{\partial r}$:

$$\frac{\partial W_{lan}}{\partial \lambda_r} = k_B T N \left[\beta + \lambda_r(\beta)' + \frac{(\beta)'}{\beta} - \frac{cosh(\beta)}{sinh(\beta)}(\beta)'\right] \tag{2.16}$$

And as presented in equation[2.12] and by $\frac{\partial \lambda_r}{\partial r} = \frac{1}{L}$, we arrive to the final form:

$$f_{lan} = \frac{k_B T N}{L}\mathcal{L}^{-1}(\frac{r}{L}) = \frac{k_B T}{l}\mathcal{L}^{-1}(\frac{r}{L}) \tag{2.17}$$

With all this approach, the strain energy function and the force related are characterized , but to implement them into the numerical model, some considerations and simplifications shall be done in order to numerically approach the inverse Langevin function. There are two main methods to approximate the inverse Langevin functions: series expansion and the so-called *Padé approximation*[18].

The first method is to consider a representation of $\mathcal{L}^{-1}(\frac{r}{L})$ based on a series expansion of Taylor series:

$$\mathcal{L}^{-1}\left(\frac{r}{L}\right) = \frac{3r}{L} + \frac{9}{5}\left(\frac{r}{L}\right)^5 + \frac{297}{175}\left(\frac{r}{L}\right)^5 + ... \tag{2.18}$$

As it can be seen, if only the first term of the expansion is taken we arrive to the Gaussian approximation.

The second method, which is the one that will be used in this work, is the rational approximation or *Padé* approximation[23]. Although there are many variations and types of considering this approximation, it is used a simple and effective one, such as:

$$\mathcal{L}^{-1}(\frac{r}{L}) = \frac{r}{L}\frac{(3 - \frac{r^2}{L^2})}{(1 - \frac{r^2}{L^2})} \tag{2.19}$$

Worm-like chain model

The Worm-like chain model(WLC) is another typical model used to describe polymer chains. Classically, the WLC has been used to characterize biological tissues, but in this work will be also used to describe rubber. As opposed to the FJC, in the WLC the directions of the N bonds of equal fixed length l are not totally free to move, that is, there is an existing bending rigidity, leading to an energy cost to overcome[32]. For this reason, these type of chains are characterized of a smooth curvature (see Figure 2.3).

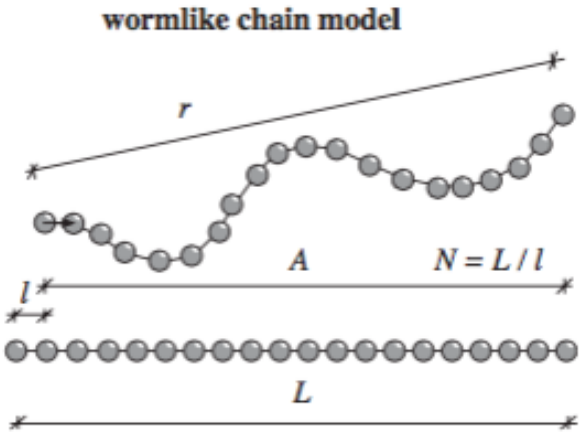

Figure 2.3: Schematic representation of a worm-like chain with all the characteristic parameters[18].

As it can be seen on the figure above, the worm-like chain model is characterized by almost the same parameters of the freely jointed model like the end-to-end distance r, the number of bonds N, the length l the contour length L. However, there is another important parameter, the persistence length A, useful to reflect this continuity explained above. Varying between $l \leq A \leq L$, the persistence length can be understood as the sum of the average projection of all bonds onto the direction of the first bond[18], and can also give information about the stiffness. For example, for the case $A \approx L$ the material is considered to act like a stiff rod, while for $A << L$ can be the case of a flexible polymer. Another case of a parameter that also gives stiffness information of the material is the Kuhn length b. This parameter can be related to the persistence length of the WLC as $b = 2A$[32], while for the FJC corresponds to the length of the links $l = b$[19].

An analytically exact expression for the force in a single chain is not available for the WLC, but there are different interpolation formula which able to determine the force[21],and so, its strain energy function related. Different interpolation formulas are presented, starting from the general form in terms of force:

$$f^{wlc} = \frac{k_B T}{4A}\left[4\frac{r}{L} + \frac{1}{\left(1-\frac{r}{L}\right)^2} - 1\right] \tag{2.20}$$

And, then, by integrating the force stretch relation above, can be obtained the strain energy function:

$$W^{wlc} = W_0^{wlc} + \frac{k_B T L}{4A}\left[2\frac{r^2}{L^2} + \frac{1}{\left(1-\frac{r}{L}\right)} - \frac{r}{L}\right] \tag{2.21}$$

This general form but with some enthalpic corrections for large strains can be also considered. Theses enthalpic corrections are mainly considered when analyzing DNA, because sometimes, there is a limiting force beyond what the DNA displays a linear behavior – in the large strain range – and these corrections are used to describe this limit behavior [31] as:

$$f^{wlc} = \frac{k_B T}{A}\left[\frac{r}{L} + \frac{1}{4\left(1-\frac{r}{L}\right)^2} - \frac{1}{4} + \sum_{i=2}^{i\leq 7}\alpha_i(\frac{r}{L})^i\right] \tag{2.22}$$

Being α_i, $i = 2, ..., 7$, are phenomenological parameters accounting to these corrections[21]. Finally, we present also a reduced variation of the WLC Eq.2.20 for which the first term $4\frac{r}{L}$ is omitted:

$$f^{wlc} = \frac{k_B T}{4A}\left[\frac{1}{\left(1-\frac{r}{L}\right)^2} - 1\right] \tag{2.23}$$

In Section 3.1.1, these variations of the WLC are going to be applied to the DNA to see their differences. Afterwards, only the standard WLC of Eq.2.20 will be used. In the case of Eq.2.23, although our purpose is not to analyze the entropic limit of the DNA, we are going to apply it anyway in order to do a better comparison.

2.2 Phenomenological models

Although the elasticity of rubber-like materials has been considered as an ideal area of application of isotropic elasticity theory, the phenomenological approach models are characterized on a general lack of a connection to the molecular structure of the material[9]. This may occur because they are formulated in the form of polynomial strain energy functions of principal stretches or invariants. These models have been used with excellent results to reproduce the macroscopic response of rubber materials, but this lack of connection to their molecular structure may not work properly for biological tissues.

Most continuum mechanics treatments of rubber elasticity stand on the fundamental basis of continuum mechanics for an isotropic, hyperelastic material. It can be characterized by the strain energy function W or by the strain energy density function $\Psi = nW$ that is usually expressed in terms of the principal invariants or the principal stretches. This can be expressed as follows:

$$\Psi = nW = nW(F) = nW(\lambda_1, \lambda_2, \lambda_3) = nW(I_1, I_2, I_3) \tag{2.24}$$

where $\lambda_1, \lambda_2, \lambda_3$ are the principal stretches and I_1, I_2, I_3 are the invariants of Cauchy-Green strain tensor ($C = F^T F$). The relation between them follows:

$$I_1 = \lambda_1^2 + \lambda_2^2 + \lambda_3^2 \tag{2.25}$$

$$I_2 = \lambda_1^2\lambda_2^2 + \lambda_2^2\lambda_3^2 + \lambda_1^2\lambda_3^2 \tag{2.26}$$

$$I_3 = J^2 = \lambda_1^2\lambda_2^2\lambda_3^2 \tag{2.27}$$

To obtain the stress-strain relation the strain energy density should be differentiated through the stretch λ. Moreover, considering that these materials are incompressible, the expression[2.27] turns out to be $I_3 = \lambda_1^2\lambda_2^2\lambda_3^2 = 1$. The stress-strain relation will be obtained as:

$$\sigma_i = \frac{\partial \Psi}{\partial \lambda_i} \tag{2.28}$$

And if the strain energy density is in terms of the invariants $\Phi = \Phi(I_1, I_2)$ must be accounted for a change of variable:

$$\sigma_i = \frac{\partial \Psi}{\partial I_1}\frac{\partial I_1}{\partial \lambda_i} + \frac{\partial \Psi}{\partial I_2}\frac{\partial I_2}{\partial \lambda_i} \tag{2.29}$$

Having done this general review of the basics of phenomenological models and before entering to the definition of these models, some considerations shall be taken in order to define the contributions to the macroscopic mechanical response.

2.2.1 Macroscopic Hyperelastic framework

Phenomenological models report for a macroscopic description of the material, thus, their strain energy density is characterized by different contributions to the macroscopic strain energy density. Taking into account the postulation of hyperelasticity, the so-called strain energy density function Ψ, for the overall network consideration, is assumed to be decoupled into different contributions:

$$\Psi = \Psi_{vol} + \Psi_{ich} \tag{2.30}$$

where $\Psi_{vol}(J)$ is the volumetric contribution, describing the strain energy associated to changes in volume. There is also the isochoric part Ψ_{ich}, which, as can be supposed, correspond to contributiona not submitted to volumetric changes($\Delta V = 0$). In this case, can also be decomposed into two different parts, isotropic and anisotropic contributions, giving a final strain energy density function defined as:

$$\Psi = \Psi_{vol} + \Psi_{ani} + \Psi_{iso} \tag{2.31}$$

This last split between anisotropic and isotropic is due to the different states of matter present in soft materials. For biological tissues, such as blood vessels, collagen or elastin, the isotropic part can be associated to the water ground substance. With the assumption of quasi-incompressibility the volumetric contribution is considered to be $\Psi_{vol}(J) = \frac{1}{D}\ln^2(J)$, being D a penalty-like parameter and $J = \lambda_1\lambda_2\lambda_3$ as in Eq. 2.27. Furthermore, two essential kinematic parameters useful to describe the elasticity of such materials may be also presented, these are the deformation gradient F and the Cauchy-Green tensor C. In terms of principal directions the deformation gradient is expressed:

$$F = \begin{bmatrix} \lambda_1 & 0 & 0 \\ 0 & \lambda_2 & 0 \\ 0 & 0 & \lambda_2 \end{bmatrix} \tag{2.32}$$

The deformation gradient contains the information about the deformation suffered by each principal direction. Then, the Cauchy-Green tensor can be defined as $\mathbf{C} = \mathbf{F}^T \cdot \mathbf{F}$.

Obtaining the isotropic contribution

The process to obtain the stress associated to the factor Ψ_{iso} is going to be done by the particular case of simple tension and incompressibility assumption as well(neglecting also the volumetric contribution by $J = 1$). Then by setting Eq. 2.32 with $\lambda_1 = \lambda; \quad \lambda_2 = \lambda_3 = \frac{1}{\sqrt{\lambda}}$ the Cauchy stress tensor defined in [21] takes the form:

$$T = -pI + 2\frac{\partial\Psi}{\partial I_1}C - 2\frac{\partial\Psi}{\partial I_2}C^{-1} \tag{2.33}$$

Being p the an arbitrary hydrostatic pressure[20] and I the identity tensor. Comment also that this formula is originally done by the left Cauchy-Green deformation tensor $\mathbf{B} = \mathbf{F} \cdot \mathbf{F^T}$ but for the case of simple tension considered results into $B = C$. In terms of the tension components Eq. 2.33 will become:

$$t_i = 2\left(\lambda_i^2\frac{\partial\Psi}{\partial I_1} - \lambda_i^{-2}\frac{\partial\Psi}{\partial I_2}\right) - p \qquad ; \qquad i = 1, 2, 3 \tag{2.34}$$

For simple tension can be recalled that $t_2 = t_3 = 0$ arriving to the conclusion that $p = 2(\lambda^{-1}\frac{\partial\Psi}{\partial I_1} - \lambda\frac{\partial\Psi}{\partial I_2})$. The derivatives of the strain energy function Ψ_{iso} with respect the first and the second invariant are then:

$$\frac{\partial\Psi}{\partial I_1} = \frac{\partial\left(\mu[I_1 - 3]\right)}{\partial I_1} = \mu \qquad ; \qquad \frac{\partial\Psi}{\partial I_2} = 0 \tag{2.35}$$

With all this at hand, one finally obtains the first tension component associated:

$$t_1 = 2\mu[\lambda^2 - \lambda^{-1}] \tag{2.36}$$

To get it in terms of nominal stress σ, there is only necessary to apply the relation $\sigma = \lambda^{-1} \cdot t$ to Eq.2.36.

2.2.2 Representative phenomenological models

As there are many phenomenological models, only some representative ones are going to be presented. One of the simplest example of these type of models would be the neo-Hookean model. As its name can indicate, this model is entirely related to the Hooke's Law. Its strain energy density function associated is equal to the isotropic contribution just obtained:

$$\Psi_{NH} = \Psi_{iso} = \mu(I_1 - 3) \tag{2.37}$$

Notice that for no deformation applied, $I_1 = 0$ and the expression would be vanished. Although it provides an accurate prediction of the material behavior at initial strain range, it results to fail at the high strain range due to the non-linearity of soft materials.

Another model that could be representative is the Mooney Rivlin model, for which its general form is expressed as:

$$\Psi = \sum_{i,j=0}^{\infty} C_{ij}(I_1 - 3)^i(I_2 - 3)^j + \frac{1}{D}(J-1)^2 \tag{2.38}$$

It is more common to use this expression accounting only for the first term. Being $I_3 = J^2 = 1$, and taking only the first term of the summation, Eq.(2.31) gets:

$$\Psi_{MR} = C_{10}(I_1 - 3) + C_{01}(I_2 - 3) \tag{2.39}$$

This model is particular for its non-dependence on the shear strain[22]. To obtain the stress-strain relation the same process as above shall be done. The advantage of these types of models is that there is one or few parameters to obtain in order to fulfill an experimental fitting parameter process. Most of times will correspond to a constant depending on the chain density $n[n^o chains/m^3]$.

Eventually, a phenomenological stretch based model will be presented. In this work one is referred to as *exponential model* because the strain energy density function is defined by a material constant k_1, a dimensionless parameter k_2 and the stretch λ expressed by an exponential relation as:

$$\Psi(\lambda_i) = \frac{k_1}{2k_2}\left[e^{\left(k_2[\lambda_i^2-1]^2\right)} - 1\right] \tag{2.40}$$

Then, the stress-strain relation can be easily obtained as:

$$\sigma = \frac{\partial \Psi}{\partial \lambda} = 2k_1\lambda_i[\lambda_i^2 - 1]^2 e^{\left(k_2[\lambda_i^2-1]^2\right)} \tag{2.41}$$

2.3 Classical Network models

In section 2.1 we have reviewed the statistics applied to a single chain and a general way to find its corresponding strain energy and force – Section 2.1 –, but, with

the aim to link the single-chain statistical theory into a network environment, now one introduces some of the classical network models. The main concept is to set a *structure* – in some contexts can be recalled as bulk – where chains can interactuate in a trivial way. Most of the classical network models consider a structure where chains are lying in order to approach the bulk structure and simplify the problem. This can be the example of the three chain model(3-CH) and eight chain model(8-CH), both consider a cubic cell that deforms accordingly with chains. Therefore, network models can be understood as a mix of a phenomenological approach of the bulk or chains environment, and the micromechanically treatment of the chains in terms of statistical mechanics just seen.

3-CH model

The three chain model is one of the simplest network models that gives a good approach of a constitutive framework necessary to relate the individual chain stretch into an overall stretch. This is accomplished assuming three sets of chains oriented in the principle directions of deformations, representing the polymer network. These chains are located in the axes of the cubic cell, permitting the whole block to deform together as shown in Figure 2.4.

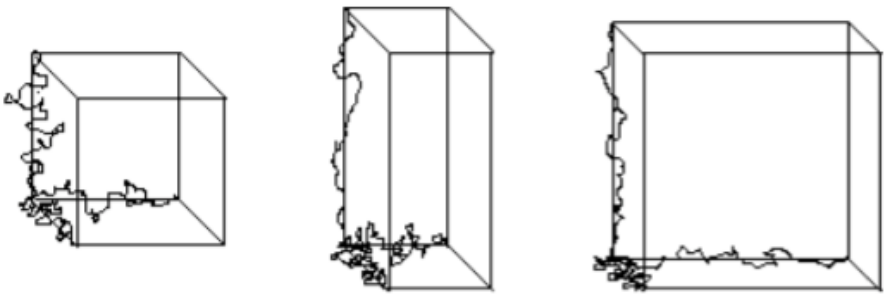

Figure 2.4: Schematic of different deformation states of the 3-chain network model. From the left to the right figure is represented the undeformed state, the uniaxial tension deformation, and the equi-biaxial tension deformation state [22].

The macroscopic strain energy density of the network is determined by the multiplication of the number of chains in the network with the arithmetic mean of the chain strain energies in the principal directions:

$$\Psi(\lambda_1, \lambda_2, \lambda_3) = \frac{n}{3} \sum_{i=1}^{3} W_{chain}(\lambda_i) \tag{2.42}$$

where n denotes the network chain density. Extending the expression above by considering the non-Gaussian statistic of the inverse Langevin, Eq.[2.35] becomes:

$$\Psi_{3ch} = \frac{nk_BT}{3}\sqrt{N} \sum_{i=1}^{3} \lambda_i \beta_i + \sqrt{N} \ln\left(\frac{\beta_i}{\sinh \beta_i}\right) \tag{2.43}$$

8-CH model

In the eight-chain model, or also called Arruda and Boyce model[22], a cubic unit cell where the chains are located along their diagonals is defined. A single network stretch is taken, which is representative for all the chains constituting the network. Accounting for the symmetry of the chain structure and assuming that the interior junction point between chains does not displace from the center of the cubic cell, the representative chain stretch $\widehat{\lambda}$ is found to be the root mean-square of the applied stretches:

$$\widehat{\lambda} = \sqrt{\frac{\lambda_1^2 + \lambda_2^2 + \lambda_3^2}{3}} = \sqrt{\frac{I_1}{3}} \tag{2.44}$$

The total strain energy density can be splitted into different contributions – See Figure 2.5 –. The bulk contribution can be identified with the isotropic contribution of Eq.2.37. Φ_{chn} is the energy related to the assembly of the chains defined by the single-chain theory just seen, and Φ_{rep} is the parameter guaranteeing the stress-free state in the reference configuration.

For the case of the inverse Langevin statistic, the strain energy density of the 8-CH model will be:

$$\Psi_{chn} = nW(\widehat{\lambda}) = nk_BT\sqrt{N}\left[\beta\widehat{\lambda} + \sqrt{N}\ln\left(\frac{\beta}{\sinh\beta}\right)\right] \tag{2.45}$$

In addition, the repulsive term that may be subtracted to this factor, being expressed as follows:

$$\Psi_{rep} = n_iKT\sqrt{N}\beta_0\ln\lambda \tag{2.46}$$

being $\beta_0 = \mathcal{L}^{-1}(\frac{r_0}{L})$ as done in [33].

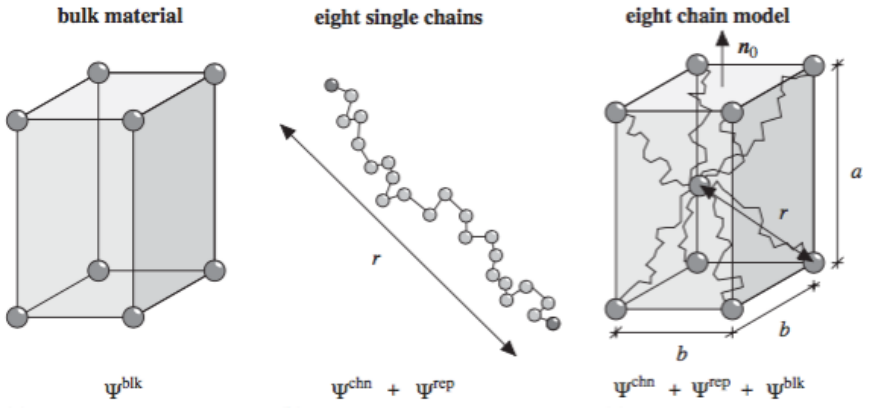

Figure 2.5: Schematic representation of the 8-CH taken from [18]

There is also usual to combine the 8-CH model within the WLC, specially in the treatment of biological tissues[18][27]. The chain contribution will the same as in Eq. 2.21 but with the consideration of the chain density n. The repulsive term Ψ_{rep} in this case is defined as:

$$\Psi_{rep} = -\frac{nk_BT}{16Ar_0}\left[\frac{4r_0}{L} + \frac{1}{[1-\frac{r_0}{L}]^2} - 1\right] \cdot \widehat{\Phi}_{rep} \tag{2.47}$$

Being the factor $\widehat{\Phi}_{rep} = \ln\left(I_4^{\frac{a^2-b^2}{2}}\right) + \frac{3}{2}\ln\left(I_1^{b^2}\right)$ where a and b are the initial dimensions of the unit cell. The ratio $\frac{a}{b}$ is representative of the degree of anisotropy [18]. One appeals to the treatment done in [26] taking into account the strain energy stored by a micro-fibre as a function of the macroscopic stretch and also considering the inclusion of the repulsive and bulk terms directly to the chain contributions. The one-dimensional case is presented as follows:

$$\Psi_f = \begin{cases} 0 & \text{if } \lambda \leq 1 \\ \frac{nKTL}{4A}\left[2\frac{r^2}{L^2} + \frac{1}{1-\frac{r}{L}} - \frac{r}{L} - \frac{\ln(\lambda^{4r_0^2})}{4r_0L}\left[4\frac{r_0}{L} + \frac{1}{[1-\frac{r_0}{L}]^2} - 1\right] - \Psi_r\right] & \text{if } \lambda \geq 1 \end{cases} \tag{2.48}$$

Being $\Psi_r = 2(\frac{r_0}{L})^2 + \frac{1}{1-\frac{r_0}{L}} - \frac{r_0}{L}$ being the constant that makes zero strain at initial conditions($\lambda = 1$). Then to obtain the stress associated, the equation 2.48 must be derived with respect to λ obtaining the final expression:

$$[\Psi_f]' = \sigma_f = \frac{nKTr_0}{4A}\left[4\frac{r_0}{L}\left[\lambda - \frac{1}{\lambda}\right] + \frac{1}{\left[1-\frac{r}{L}\right]^2} - \frac{1}{\lambda\left[1-\frac{r_0}{L}\right]^2} + \frac{1}{\lambda} - 1\right] \tag{2.49}$$

2.4 Full-Network models

2.4.1 Micro-Sphere Based Model

As the Classical Network models just presented, Full-Network models not only combine the micro-mechanically treatment of chains with the implementation of a network structure, but also gives and exhaustive approach by considering a representative volume element that contains an averaging of the distribution of the micro-kinematic variables to extend them to the macro-scale quantities[24]. The essence of these models, in particular the micro-sphere based model, is the definition of a unit micro-sphere, from where integrating along its surface and by different integration directions, the overall response of the network can be obtained. In this work the case of an unconstrained network is only treated. That means that physical entanglements creating constrains between chains are not considered.

Micro-Sphere Setting

This model assumes the same split of the strain energy density as in Eq. 2.31. The difference is that Ψ_{ani} is computed for all integration directions and with the inclusion of anisotropy, if necessary. To compute Ψ_{ani}, there is the need to define the parameters regarding to the micro-sphere from which, by integrating over its

surface among m orientation directions $\{\mathbf{r}^i\}_{i=1...m}$ of chains (Fig.2.6), the whole mechanical response will be obtained. Moreover, given the orientation vectors r and the deformation gradient, the vector t can be defined as:

$$t = F \cdot r \qquad being \qquad ||t|| = \lambda \tag{2.50}$$

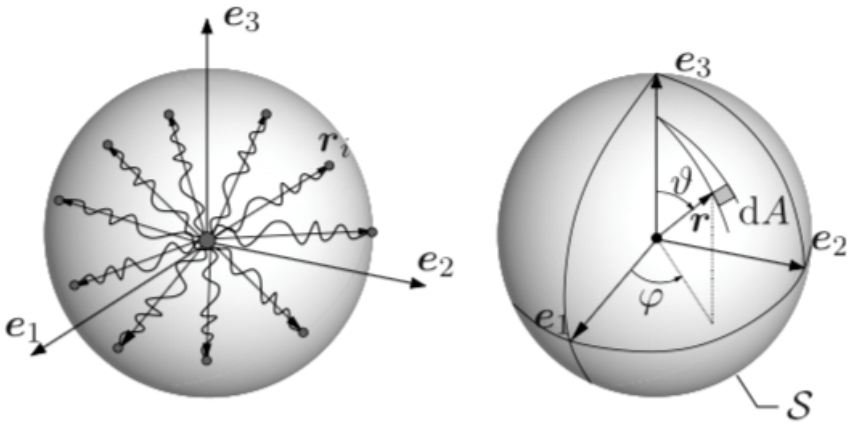

Figure 2.6: Schematic representation of the micro-sphere based model[25]

Considering the unit sphere $\mathcal{S}^2$, a discretization into these m orientation vectors shall be done within the weighting factors $\{v^i\}_{i=1...m}$.Then the integral over the unit sphere $\mathcal{S}^2$ can be approximated as[26]:

$$\langle(\bullet)\rangle = \frac{1}{4\pi}\int_{\mathbb{U}^2}(\bullet)\mathrm{dA} \approx \sum_{i=1}^{m} v^i(\bullet)^i \tag{2.51}$$

With this basic framework,the strain energy function can be now implemented in the micro-scale to obtain the one associated into the overall network. Then, the anisotropic contribution related to the fibers of the material, can be expressed as:

$$\Psi_{ani} = \sum_{j=1}^{N}\Psi_f^j = \sum_{j=1}^{N}\left[\frac{1}{4\pi}\int_{\mathbb{U}^2} n\rho_{\mathrm{f}}W_{\mathrm{f}}dA\right] \tag{2.52}$$

being N the families of fibers in the anisotropic part, Ψ_f^j as the strain energy function associated to this j-nth family, ρ_{f} a statistical value related to the fiber dispersion and anisotropy – obtained by the ODFs – and W_f the strain energy function of the fiber-level.

Then, by the discretization exposed in Eq.2.51, the strain energy density function related to the anisotropic part Eq.2.52 takes the final form:

$$\Psi_{ani} = \sum_{j=1}^{N}\left[\sum_{i=1}^{m} n\rho_i v^i W(\lambda_i)\right] \tag{2.53}$$

Finally, deriving the strain energy function of the fiber-lever W_f with respect to the stretch λ, the stress contribution for a family of fibers can be obtained. This macroscopic contribution is commonly described in terms of Kirchhoff stresses giving:

$$\tau_f = J\sigma_f = \left\langle (n\rho W_f' \lambda_f^{-1} \bar{t} \otimes \bar{t}) \right\rangle = \sum_{i=1}^{m} \left[n\rho_i W_i' \lambda_f^{-1} \bar{t} \otimes \bar{t} \right] v^i \tag{2.54}$$

Being W_f' the first derivative of W with respect to λ_i. For an incompressible material $J = 1$ the Kirchoff stresses and the Cauchy stresses components will be equal($\tau_f = J\sigma_f$). Finally, the term W_f can be computed with the models commented in Chapter 2, i.e. the WLC model or the FJC model.

Inclusion of anisotropy

Most of biological soft tissues – such as cardiovascular tissues – present, in certain bundles of fibers, a preferential direction that appeal to the anisotropy of the material. For the inclusion of anisotropy into the micro-sphere based models, there is the need to define an ODF permitting to account for the distribution and dispersion of such fibrils/fibers. The Bingham distribution is adopted to compute the parameter ρ that depends on three different concentration parameters $\kappa_{1,2,3}$ in three orthogonal directions in space, making easier to correlate these orientations to the main directions accounted for biological tissues: axial, radial and circumferential. The Bingham ODF is characterized to be antipodally symmetric in the unit micro-sphere $\mathcal{S}$ – opposite points have equal probability – [34].

For the definition of the Bingham ODF one has followed the scheme in [27], starting with the following expression:

$$\rho(r;\, A)\, \frac{\mathrm{d}A}{4\,\pi} = \left[K(A)\right]^{-1} \exp\left(r^{\mathrm{t}} \cdot A \cdot r\right) \frac{\mathrm{d}A}{4\,\pi}, \tag{2.55}$$

where A is a symmetric $3x3$ matrix, $\mathrm{d}A$ is the Lebesgue invariant measure on the unit sphere, $r \in \mathcal{S}^2$ and $K(A)$ is a normalizing constant. Applying some transformations, Eq. 2.55 can be rewritten as

$$\rho(r;\, Z,\, Q)\, \frac{\mathrm{d}A}{4\,\pi} = \left[F_{000}(Z)\right]^{-1} \operatorname{etr}\left(A \cdot A^{\mathrm{t}} \cdot r \cdot r^{\mathrm{t}} \cdot Q\right) \frac{\mathrm{d}A}{4\,\pi}, \tag{2.56}$$

where $\operatorname{etr}(\bullet) \equiv \exp(\operatorname{tr}(\bullet))$, Z is a diagonal matrix with eigenvalues $\kappa_{1,2,3}$, $Q \in \mathbb{Q}^3$ such that $A = Q \cdot Z \cdot Q^{\mathrm{T}}$ and $F_{000}(Z)$ may be written as

$$F_{000}(Z) \,=\, \left[4\,\pi\right]^{-1} \int_{\mathcal{S}^2} \operatorname{etr}\left(Z \cdot r \cdot r^{\mathrm{t}}\right) \mathrm{d}A \tag{2.57}$$

In the application of the micro-sphere based model – Section 3.2.2 –, the eigenvalues $\kappa_{1,2,3}$ and the orientation matrix Q used, has been extracted from [36]. With the distribution fiber factor ρ defined, there is only the need to compute the strain energy related to fibers, that will depend of the model chosen, being able to reproduce the behavior of the whole network.

2.5 Fitting material parameters with experimental data

The models explained in Chapter 2 are able to represent in a quite accurate manner the behavior of such materials, but there is the need to present the fitting process for which these models can be tested with experimental data. Thus, material's behavior could be recalled by extrapolating its characteristic material parameters.

The main goal is to minimize the difference between the experimental data and the results obtained from the model, in a least-square scheme as follows:

$$\mathcal{X}^2 = (\sigma_{model} - \sigma_{data})^2 \tag{2.58}$$

The parameter σ corresponds to the stress σ, force f or normalized force depending of the magnitudes working in each case. By this scheme, this functional is optimized permitting the experimental curve obtained from the models to fit the points extracted from the experimental data. Then, the Normalized Mean Square Error(NRMSE)[27] is also computed, giving a statistic representation of the error inherent to the process:

$$NRMSE = \frac{\sqrt{\frac{\mathcal{X}^2}{p-q}}}{\nu} \tag{2.59}$$

With:

$$\nu = \frac{1}{p}\sum_{j=1}^{p}[\sigma_{model} + \sigma_{data}] \tag{2.60}$$

Being p the number of the parameters to be fitted, and q the number of parameters to be identified – constants of the model – , so that $p - q$ is the number of degrees of freedom. Also, can be considered ν as the mean of the parameters calculated by the model. The functional in Eq. 2.58 will be optimized using the *Matlab* tool *fmincon*, by a domain or a range of values for which the function is evaluated until a minimum is found.

And so, by this main scheme, some experimental data will be fitted and some parameters regarding to the material, like the contour length L or the persistence length A, will be obtained from force-extension data.

3 Results

The WLC and the FJC models will be applied to rubber and biological tissues at different scales. Special treatment will be given to cardiovascular tissue components such as collagen and elastin contained in human beings. In order to make a smooth transition to the Full-Network models, micro-mechanically based models are going to be applied first, followed by classical network models, ending with the intensive computation of the Micro-Sphere based models of the cardiovascular tissue, made of a network of collagen and elastin fibers.

3.1 Mechanics of micro-structural components

3.1.1 Stretching DNA

Before studying the cardiovascular tissue, we considered to characterize the mechanical behavior of one of the most elementary molecules in biology: DNA. Force-extension experimental data from Smith[28] has been used for model testing. It is distinguished between a larger DNA chain and a smaller one, that from now on, are going to be treated as Specimen A and Specimen B respectively. As the data from Smith is expressed in terms of force[pN]-extension[μm], the minimization of the functional Eq.2.58 will be done for the parameter force f instead of stress σ. Said that, both WLC and FJC are going to be confronted to this experimental data.

The WLC model consists of a two-parameter characterization, accounting for the persistence length A and the contour length L. All three forms or variants of the WLC expressed in Eqs.2.20,2.22,2.23 are going to be tested with the aim to see its applicability and to perceive differences between them. In Figure [3.1] can be seen the fitting of the experimental data of Eq.2.20 for Specimens A and B. The figures corresponding to the fitting for Eqs.2.22,2.23 are not included because there are no significant differences between them. In tables 3.1 and 3.2 are summarized the values of the characteristic material parameters obtained from the fitting process, as well as the error ϵ for both specimens and the three variations of the WLC. Comment that one has considered a temperature equal to $T = 293K$

and the Boltzmann constant $k_B = 1.38 \cdot 10^{-23}[J/K]$ in all cases.

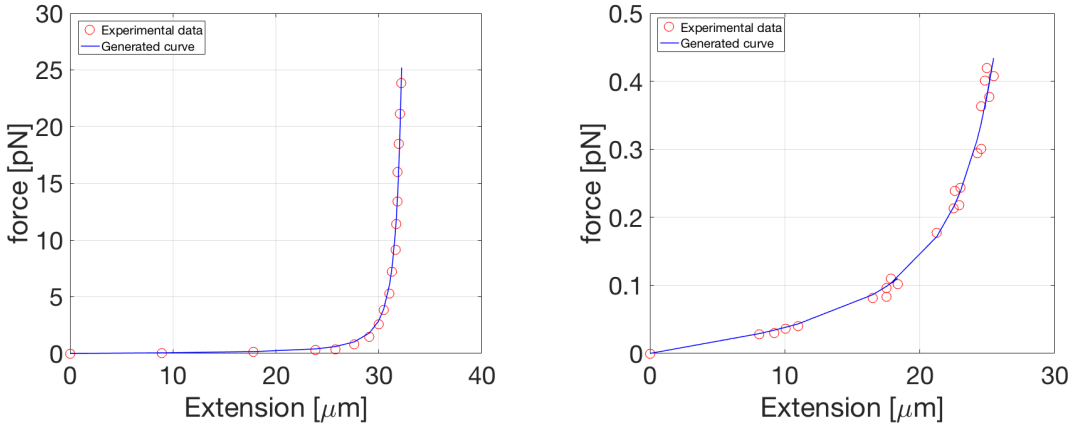

Figure 3.1: Force-extension relationship of DNA, specimen A(left) and specimen B(right). Solid lines represent the theoretical fitting according to the WLC (Eq.2.20), and "o" are the experimental data points extracted from Smith. [28]

Table 3.1: Fitting parameters, specimen A

WLC-specimen A	A[μm]	L[μm]	ϵ[-]
standard[2.20]	0.0361	33.3152	0.1140
reduced[2.22]	0.0351	33.3299	0.1097
enthalpic corr[2.23]	0.0354	33.3251	0.1103

Table 3.2: Fitting parameters, specimen B

WLC-specimen B	A[μm]	L[μm]	ϵ[-]
standard[2.20]	0.0630	31.8544	0.1059
reduced[2.22]	0.0356	33.9591	0.1049
enthalpic corr[2.23]	0.0524	32.2984	0.1063

In view of the results, there is not a relevant difference between WLC variations regarding to the fitting error. For what remains to the obtained parameters, while Specimen A do not show much variations in the material parameters, Specimen B has larger variations. Said that, can be also seen as the contour length L accounts for the maximum extensibility of these chains(specially for Specimen A), making the f tending to infinity as the values of r approach L.

For the case of the FJC, the non-Gaussian approach of the inverse Langevin will be used as presented in Eq.2.17. The parameters to be fitted in this case will be the contour length L and the other might be N or l. As $L = Nl$, there is no difference by choosing one or the other. In Figure [3.2], the result of the fitting process by the FJC is presented. Moreover, the material parameters obtained are summarized in Table 3.3.

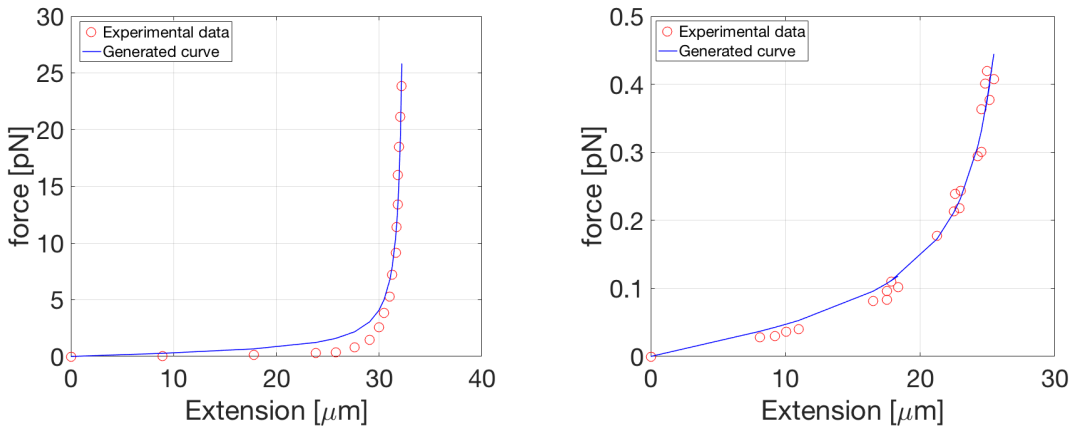

Figure 3.2: Force-extension relationship of DNA, specimen A(left) and specimen B(right). Solid lines represent the theoretical fitting according to the FJC (Eq.2.17), and "o" are the experimental data points extracted from Smith. [28]

Table 3.3: Material parameters for the FJC

FJC	L(μm)	N	l(μm)	$r_0(\mu m)$	ϵ
Specimen A(large DNA)	32.6067	2564.4307	0.0127	0.6439	0.1936
Specimen B(small DNA)	28.2006	280.8010	0.1004	1.6829	0.1204

As carrying out the fitting scheme for both models and the same experimental data, several differences can be observed. In terms of the fitting error ϵ the WLC model has better described the material behavior, getting mean values of $\epsilon_A = 0.1113$ and $\epsilon_B = 0.1057$ for Specimens A and B respectively, while for the FJC these values have resulted to be bigger, specially for the Specimen A. The other characteristic parameter that can be compared is the contour length L. Thus, the mean values for the WLC have turned out to be $L_A = 33.3234$ and $L_B = 32.7039$.

The Gaussian statistic for the FJC is only able to describe the initial linear range, missing in the non-linear part. That was the reason for which one considered the inverse Langevin statistic that has been able to capture the phenomena of strain-stiffening. Accounting for the inextensibility of the chain, strain-stiffening can be appreciated in both Specimens' curves, specially in the larger DNA chain.

3.1.2 Collagen and Elastin

Biological tissues, in special the cardiovascular tissue – collagen and elastin – are hierarchically structured, from molecules to tendons or fascicles. For this reason, may be interesting to analyze these elements at different scales, e.g. tropocollagen versus collagen fibril. Single-chain models are going to be used to characterize their micro structural components. Then, for what remains to experimental data, an uniaxial tensile test of tropocollagen has been recalled from Bozec[35]. Analogously, experimental data of uniaxial tensile tests of collagen fibrils from Eppell

[30] have also been extracted. In the fibril-scale, a macroscopic treatment will also done and compared with the single-chain models application.

Stretching TC molecules

First of all, the smallest element of collagen, the tropocollagen molecules has been analyzed. In the experimental data extracted from Bozec[35], the deformation was in terms of extension $r[nm]$ and the force in the magnitude of pN, similar as in the case of DNA. Then, Figure 3.3 shows the result to the fitting scheme for tropocollagen with the WLC and the FJC, respectively.

For the WLC, the persistence length A and the contour length L are the parameters to fit. The procedure to follow was, then, analogous to the DNA. For the FJC, the parameters to fit were the contour length L and the length of the link l. The values of parameters resulted of these applications are summarized in Table 3.4.

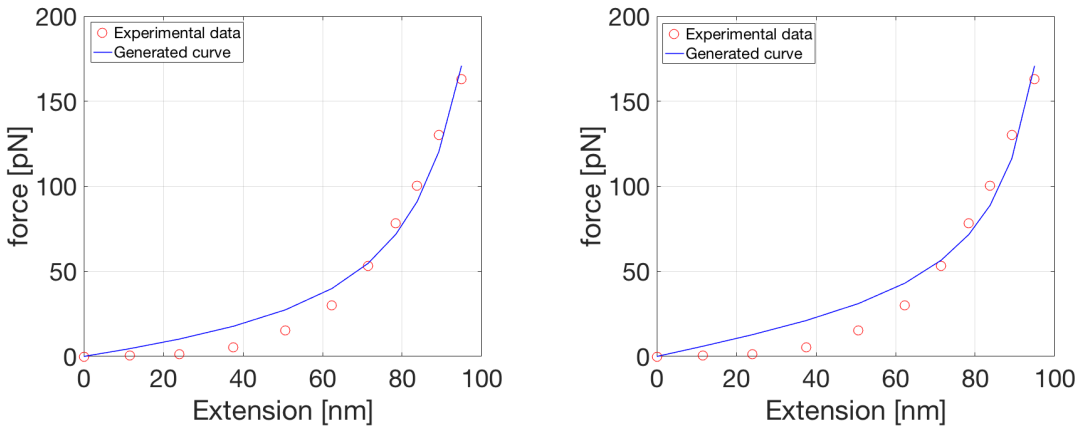

Figure 3.3: Force-stretch and force-extension relationships of tropocollagen molecules. Solid lines represent the theoretical fitting according to the WLC (Eq.2.20-left figure) and the FJC (Eq.2.17-right figure) , and "o" are the experimental data points extracted from Bozec[35].

Table 3.4: Material parameters of tropocollagen molecules for the WLC and the FJC.

Tropocollagen	L$[nm]$	A $[nm]$	N [-]	l$[nm]$	$r_0[nm]$	ϵ [-]
WLC	122.0259	0.1322	-	-	-	0.1890
FJC	106.7997	-	483.2676	0.2210	4.8582	0.2404

In terms of the values obtained, the WLC seem to give again a smaller error. Notice that as explained in Section 2.1.2, the persistence length of the FJC can be assumed equal to l. Said that, the persistence length for the FJC of this tropocollagen molecule is nearly twice of the one obtained for the WLC. This fact

is reflected in the maximum extensibility or L. As the FJC described a stiffer chain, its corresponding contour is smaller than in the WLC. Otherwise, although the FJC offered a less accurate fitting, it was able to obtain the information of all the material parameters. As the parameters to fit were L and l, can be directly obtained N, and then, by the particular relation $r_0 = \sqrt{N}l$ all the information about the material is obtained.

Stretching Collagen and Elastin fibrils

Once it has been seen the application of the WLC and the FJC into the mechanical behavior of molecules, the same methodology will be used with the upper scale-level, collagen fibrils. Two Specimens are distinguished from the data of Eppell[30], one of an initial gauge length of $r_0 = 20\mu m$ and other of $r_0 = 5\mu m$, from now on called *Specimen A* and *Specimen B*, respectively. Experimental data is expressed in μN for the force, and the *extension* axis is expressed in terms of $\Delta r = r - r_0$ [See Figure 3.4]. In this case, as one has information about r_0, extension data can be easily converted into stretch by $\lambda = (\Delta r + r_0)/r_0$.

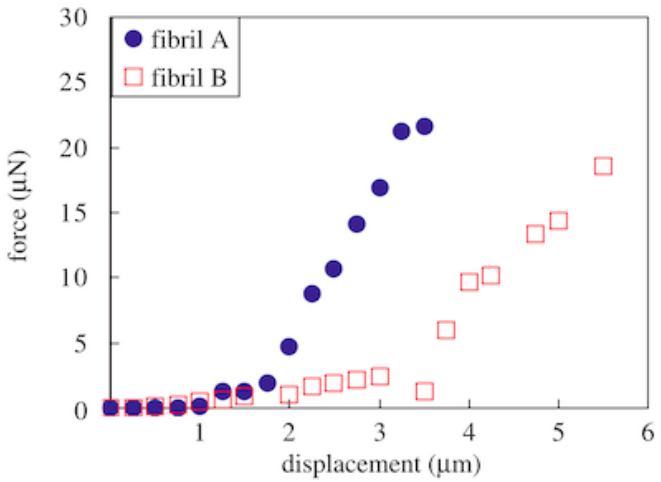

Figure 3.4: Uniaxial tension experimental data of collagen fibrils extracted from Eppell[30].

Converting the experimental data into a stretch description of the extension, and also having information about r_0, the parameters to fit get reduced. For the FJC, can be fitted only for N or l. The WLC continues to be a two-parameter model, choosing the persistence length A and the number the contour length L as the material parameters to fit. For the FJC, the other characteristic parameters can be obtained within the relations $L = Nl$ and $r_0 = \sqrt{N}l$.

Figure 3.5 and 3.6 show the results of the application of the WLC and FJC as done before. In Tables 3.5 and 3.6, the parameters obtained for each model are summarized.

In view of the results, many discrepancies can be observed. In the case of the FJC, Specimen B and, specially Specimen A, clearly do not fit as good as

expected. This fact makes one to start thinking that something may not be working accurately. For the WLC, the persistence length A is much orders of magnitude smaller than l.

Subsequently, a reason to understand this possible discrepancy may be no more that one of the main purposes of this work: to understand that these types of materials, due to their complex structure exhibit different qualitatively behavior when compared at different scales. And that is why tropocollagen, the smallest scale in the hierarchical classification, can be quite well reproduced by the single chain models. Collagen fibrils are formed of many chains of at smaller scale, making effective the need of network models to fit their parameters.

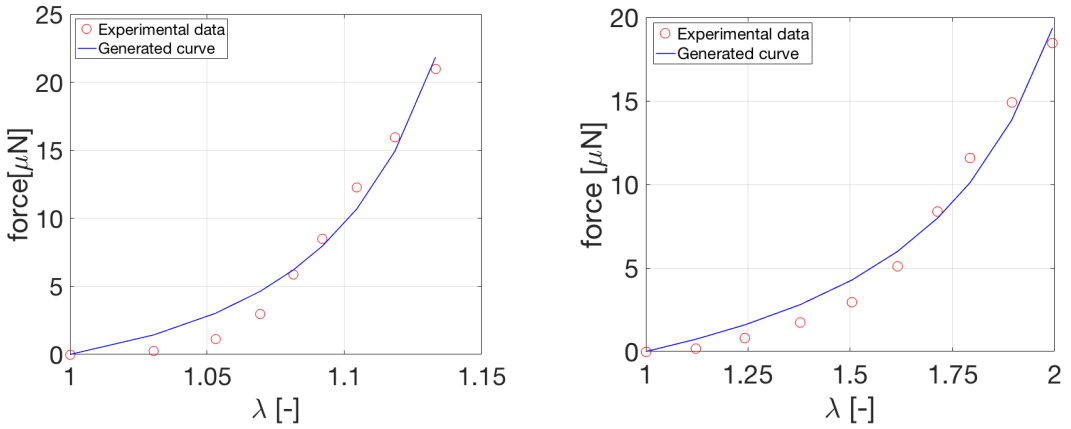

Figure 3.5: Force-stretch relationship of collagen fibrils, specimen A(left) and specimen B(right). Solid lines represent the theoretical fitting according to the WLC (Eq.2.20), and "o" are the experimental data points extracted from [30].

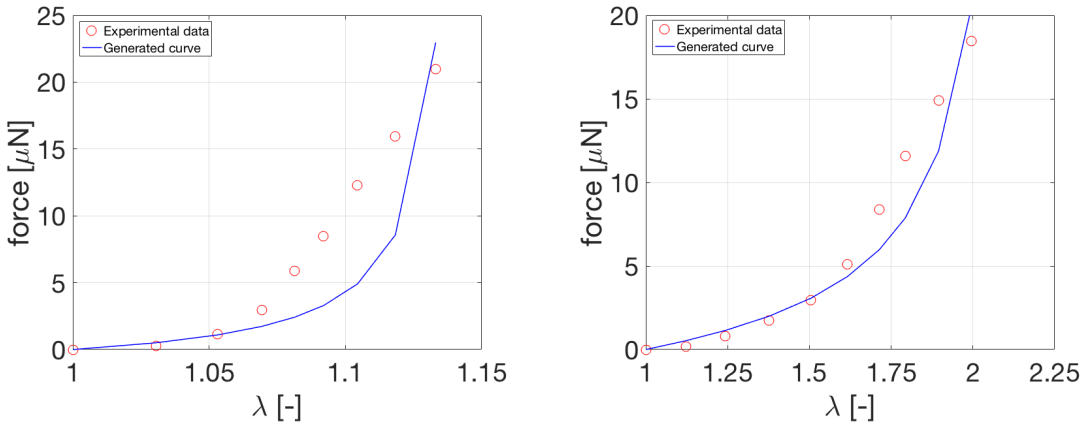

Figure 3.6: Force-stretch relationship of collagen fibrils, specimen A(left) and specimen B(right). Solid lines represent the theoretical fitting according to the FJC (Eq.2.17), and "o" are the experimental data points extracted from [30].

Table 3.5: Material parameters of collagen fibrils for the WLC

WLC	L[μm]	A [pm]	N [-]	l [μm]	ϵ[-]
Specimen A	24.4286	0.0075	1.4919	16.3743	0.1918
Specimen B	13.0685	0.0087	6.8315	1.9129	0.1747

Table 3.6: Material parameters of collagen fibrils for the FJC

FJC	L[μm]	N [-]	l [μm]	ϵ[-]
Specimen A	22.8761	1.3083	17.4855	0.6701
Specimen B	10.8117	4.6757	2.3123	0.3404

Therefore, to conclude with the proper characterization of single collagen, the same experimental data converted into stress-strain is going to be used (See Figure 3.7). Notice that the data is expressed in terms of eulerian strain – defined as $\lambda = \frac{1}{\sqrt{1-2e_{eul}}}$ – and stress reaching the order of MPa.

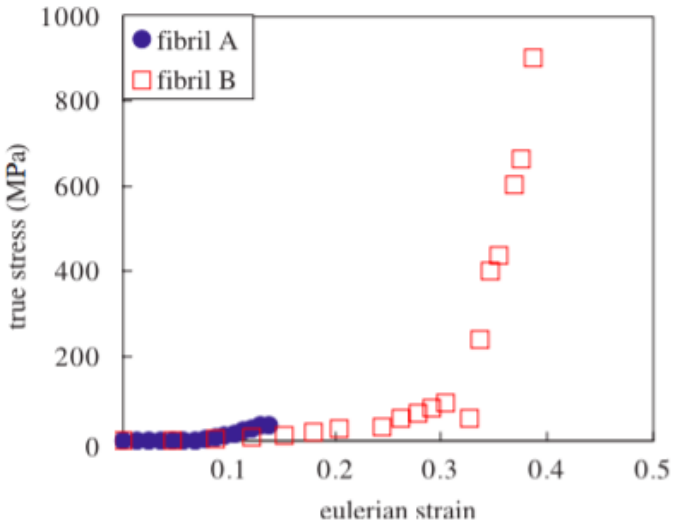

Figure 3.7: Stress-strain experimental data of collagen fibrils extracted from Eppell[30].

First the 8-CH model within the WLC following the scheme of Eq.2.49 has been applied. A two-parameter fitting process has been followed by taking the length of the link l and $B = nKTr_0/l[MPa]$ as the parameters to estimate. In order to simplify the relation between FJC and the WLC, the relation $b = 2A$ and $r_0 = \sqrt{N}l$ is assumed to be fulfilled for the WLC. Then, Eq.2.49 has been rewritten as:

$$\sigma_f = B\left[4\frac{l}{r_0}\left[\lambda - \frac{1}{\lambda}\right] + \frac{1}{\left[1-\lambda\frac{l}{r_0}\right]^2} - \frac{1}{\lambda\left[1-\frac{l}{r_0}\right]^2} + \frac{1}{\lambda} - 1\right] \tag{3.1}$$

Being $B = \frac{nk_BTr_0}{2b}$ in this case. The relative stretch λ_r has been expressed in terms of $\lambda_r = \frac{\lambda}{\sqrt{N}} = \lambda\frac{l}{r_0}$ because the undeformed chain length is known. The stress only depends of the two material parameters to estimate, B and l. Figure 3.8 shows the result of the fitting procedure using Eq. 3.1 with a clearly more accurate adjustment than done before.

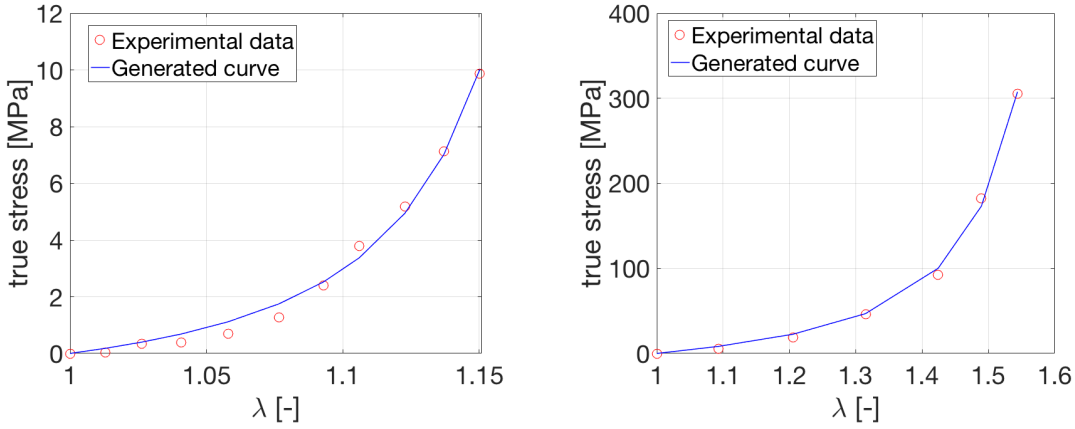

Figure 3.8: Stress-stretch relationship of collagen fibrils, specimen A(left) and specimen B(right). Solid lines represent the theoretical fitting according to the 8CH-WLC (Eq.3.1), and "o" are the experimental data points extracted from [30].

At first glance, this approach not only fits qualitatively better than those done previously, but the values obtained make physical sense – Table 3.7 –. The values of l and N fulfill the relations with the initial length known, and the square-root of N seem to approach the maximum extensibility as in Eq.2.5.

Table 3.7: Material parameters of collagen fibrils for the 8CH-WLC

8CH-WLC	B[MPa]	l[μm]	N[-]	ϵ[-]
Specimen A	0.0446	16.2855	1.5082	0.1122
Specimen B	3.1053	2.9166	2.9389	0.0699

Analogously, it has been tried to reproduce the stress-stretch curves of both specimens but considering a FJC. This modification considers the 8CH model for the FJC as in Eqs. 2.45,2.46. The stress-stretch relation is obtained by deriving the strain energy density function as:

$$\sigma = \frac{\partial \Psi}{\partial \lambda} = \frac{nk_BTr_0}{l}\left(\beta - \frac{\beta_0}{\lambda}\right) \tag{3.2}$$

So, by taking again l and the factor $B = nk_BTr_0/l$, and deriving the new strain energy associated, the values in Table 3.8 and the Fig.3.9 are obtained. As in the 8CH-WLC, the 8CH-FJC model reproduces in a more accurate manner the behavior of such specimens, confirming the hypothesis that there was the need to use network models into these collagen fibrils.

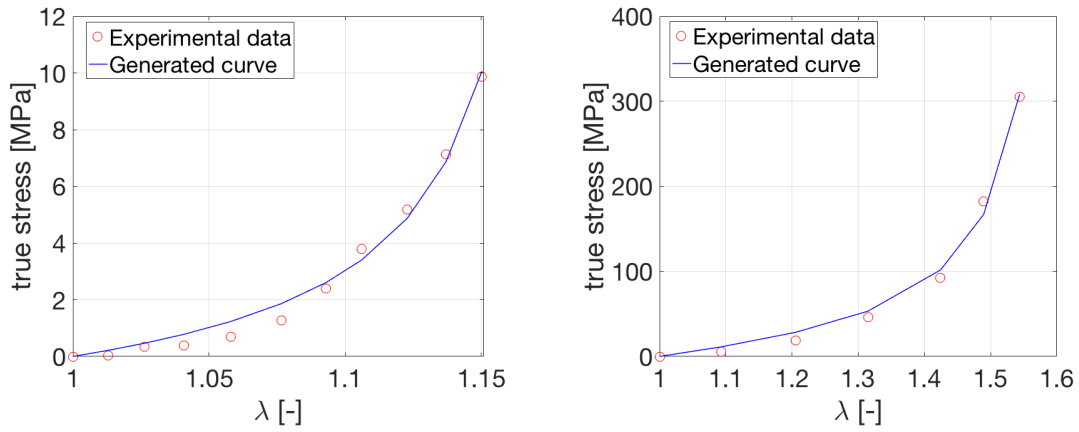

Figure 3.9: Stress-stretch relationship of collagen fibrils, specimen A(left) and specimen B(right). Solid lines represent the theoretical fitting according to the 8CH-FJC (Eqs.2.45,2.46), and "o" are the experimental data points extracted from [30].

Table 3.8: Material parameters of collagen fibrils for the 8CH-FJC

8CH-FJC	B[MPa]	l[μm]	N[-]	ϵ[-]
Specimen A	0.3771	16.8437	1.4099	0.1394
Specimen B	14.6929	3.0932	2.6128	0.1204

Finally, both network models has been applied to reproduce the behavior of elastin fibrils, a component that commonly acts in cooperation with collagen. Experimental data of an uniaxial test of elastin has been taken from [33], but it has been only taken in consideration until $\lambda \approx 1.1$. That is because in the application of the Full-Network models that will be done afterwards, is going to be considered a network of collagen and elastin acting together, and can be assumed that elastin works until these values of stretch – then starts to work the part of collagen –. Thus, in Fig. 3.10 can be seen that the behavior of elastin until $\lambda \approx 1.1$ can be considered linear. In Table 3.9 the values corresponding to an adjustment for N and B are summarized.

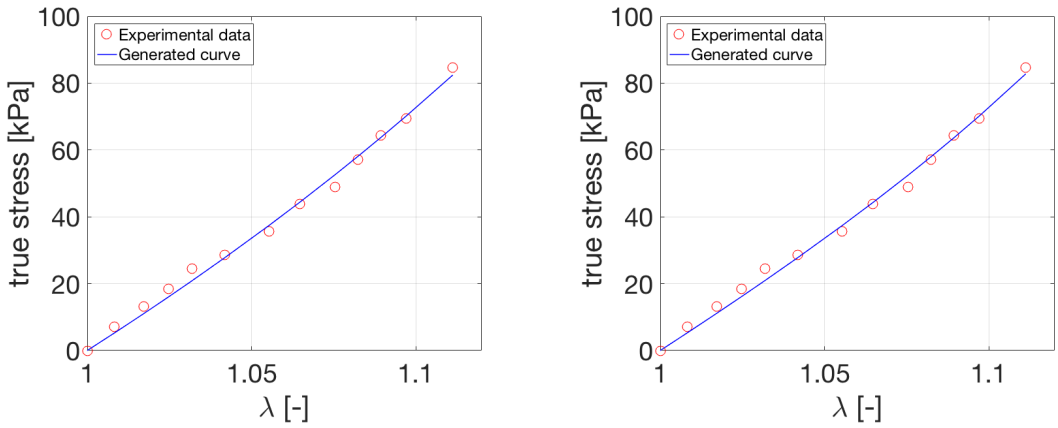

Figure 3.10: Stress-stretch relationship of elastin fibrils. Solid lines represent the theoretical fitting according to the 8CH-WLC(left figure, Eq.3.1) and 8CH-FJC (right figure, Eqs.2.45,2.46), and "o" are the experimental data points extracted from [33]

Table 3.9: Material parameters of elastin fibrils for 8CH-FJC and 8CH-WLC

Elastina	B[kPa]	N[-]	ϵ[-]
8CH-FJC	22.2380	1.8223	0.0567
8CH-WLC	39.8553	2.8005	0.0594

3.2 Macroscopic mechanical behavior

We have just analyzed the micro-structural components of biological tissues by single chain models, ending with a macroscopic treatment with the 8CH model that has improved the inaccuracy at the fibril-scale. But when looking at the macro-scale, for a network composed of many micro-structures (molecules, fibrils, etc.), its macroscopic response may be characterized through different material parameters than in the micro-scale. For this reason, now it is time to analyze the macroscopic response of soft materials, starting with an example of a rubber material and ending with the application of the Full-Network models into the cardiovascular tissue.

3.2.1 Rubber materials

In the case of rubbers, applying single chain models makes no sense since their structure do not approach the hierarchical structure of biological tissues. Then, the typical S-shaped curve of rubbers will be modeled accounting for network models.

Therefore, one considers the eight-chain model combined with the FJC and the WLC as done previously for collagen and elastin fibrils. As a result, Figure 3.11 accounting for the experimental data of Treloar [20], reproduces in a quite accurate manner the behavior of rubber. Even the initial part is not captured at all – more accentuated for WLC – , both models seem to approach exhaustively the final high strain range.

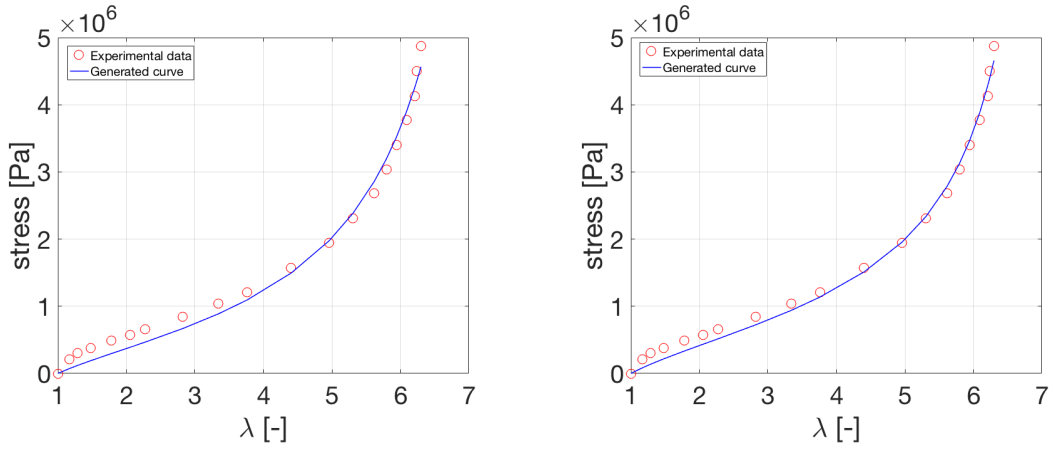

Figure 3.11: Stress-stretch relationship of a rubber-like material. Solid lines represent the theoretical fitting according to the 8CH-WLC(left figure, Eq.3.1) and 8CH-FJC (right figure, Eqs.2.45,2.46), and "o" are the experimental data points extracted from [20].

Since the deformation measure is expressed in terms of the stretch ratio and using the same relation for the persistence length than done in the fibril-scale fitting, a two-parameter fitting scheme has been carried out for the 8CH-FJC and 8CH-WLC, taking B and N as the parameters to be obtained. Looking at Table 3.10, can be seen as the FJC has better adjusted the experimental data than the WLC.

Table 3.10: Material parameters of a rubber-like material for 8CH-FJC and 8CH-WLC

	B[kPa]	N[-]	ϵ[-]
WLC	297.6451	74.8356	0.0909
FJC	633.7231	53.7765	0.0688

3.2.2 Cardiovascular tissue

For the application of the Full-Network models, attention in Cardiovascular tissues such as vessels and arterial tissues will be paid. These soft tissues are mainly composed of an ECM formed by an isotropic ground substance – with a high water content– and a network of collagen and elastin fibers[26][27]. The data from [27] accounts for simple tension tests of arterial tissue with the particularity

of not only having information about the longitudinal direction, but also in the circumferential direction. So, the micro-sphere approach is going to be used to recall their characteristics parameters, but to implement the micro-sphere based model, two deformation gradients will be taken, one for the longitudinal direction and other for the circumferential direction, both defined as:

$$F_{lon} = \begin{bmatrix} \lambda & 0 & 0 \\ 0 & \frac{1}{\sqrt{\lambda}} & 0 \\ 0 & 0 & \frac{1}{\sqrt{\lambda}} \end{bmatrix} \qquad and \qquad F_{circ} = \begin{bmatrix} \frac{1}{\sqrt{\lambda}} & 0 & 0 \\ 0 & \frac{1}{\sqrt{\lambda}} & 0 \\ 0 & 0 & \lambda \end{bmatrix} \tag{3.3}$$

The distinction between both deformation gradients is entirely related to the anisotropy and fiber dispersion since we have got information about the collagen concentration[36]. Alternatively, elastin can exhibit linear elasticity up to a stretch of $\lambda \approx 1.1$, and as it can be distributed randomly along all the unit sphere, its contribution can be associated to both stretching directions. Here is the point from which different considerations will be taken into account.

These considerations are divided into two main blocks: the first one assumes the contribution of the elastin in its first linear range ($\lambda \approx 1.1$), considering the additive decomposition of Eq.2.31 for which Ψ_{iso} is going to be defined by a Neo-hookean description.

In the second block the elastin contribution is going to be considered isotropic, but is going to be added into the integration scheme. Many sub-cases are also considered here because the material parameters obtained in Section 3.1.2 will be tested. Notice that for both blocks the collagen contribution considered is the same, always computed with the parameter ρ obtained by the Bingham distribution.

But before entering to these hypothesis about the elastin contribution, we are going to describe first the anisotropic contribution of collagen.

Collagen anisotropic contribution

First of all, to compute the collagen anisotropic contribution we have taken the parameters accounting for the collagen dispersion from[36]. They obtained the concentration parameters κ for collagen and the orientations Q from experimental tests. With this information at hand, we realized that collagen was almost entirely concentrated in the circumferential direction, as Figure 3.12 shows.

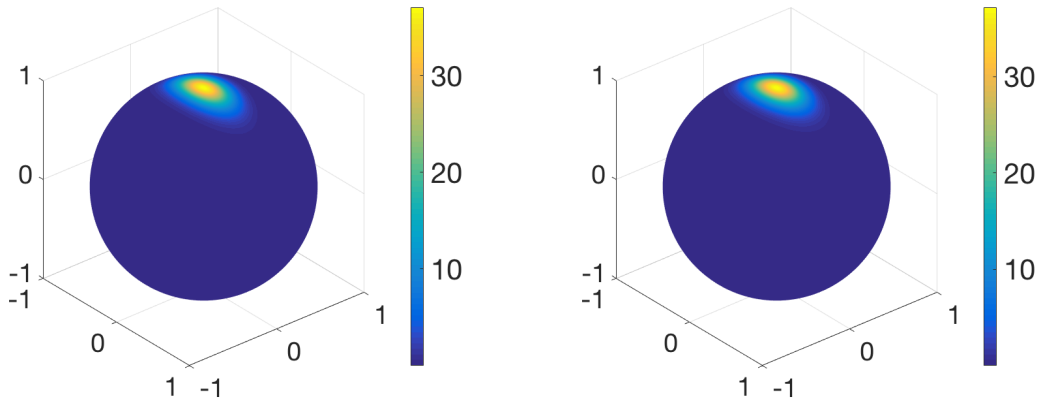

(a) $\kappa_1 = 18.6352$, $\kappa_3 = 30.6039$ (b) $\kappa_1 = 15.4663$, $\kappa_3 = 28.4003$

Figure 3.12: Representation of the ODF for different concentration parameters κ_1 – κ_3 both with $\kappa_2 = 0$ obtained from [36].

Then, to compute the anisotropic part corresponding to collagen fibers with the micro-sphere approach, we first obtain the factor ρ associated to the fiber dispersion. A Bingham ODF will be used as defined in Eqs.2.55, 2.56. The values of $\kappa_{1,2,3}$ able to get the diagonal matrix Z. Therefore, we are now available to obtain also the factor F_{000} following Eq.2.57. Within the information of the orientation of the fibers given from Q, the factor ρ can be finally obtained.

Once this term is defined, the parameters related to the discretization of the micro-sphere $\mathcal{S}^2$ shall be defined. For what remains to the weighting factors $v^i_{i=1...m}$ and the directions of integration $r^i_{i=1...m}$, a 184-points scheme has been taken. The tangent vector t and also the isochoric stretch λ can be obtained as in Eq.2.50. Finally, defining the strain energy density – with the FJC and the WLC – and deriving it with respect to the stretch, the stress contribution of the collagen is totally defined.

To obtain the total stress-stretch behavior of the cardiovascular tissue, the elastin contribution shall be added, returning to the considerations exposed at the beginning of this section.

Elastin Neo-Hookean contribution

In the first consideration, the elastin contribution to the network is considered to be isotropic, recalling its behavior from a Neo-Hookean description as in Eq.2.37. The anisotropic part will be entirely attributed to collagen, giving the total strain energy density to be divided as in Eq.2.31. The volumetric part will be neglected as the assumption of incompressibility. Said that, a previous adjustment must be done before entering to the macro-approach of the whole network. This will be the estimation of the corresponding term μ, that will be obtained from fitting only up to values of $\lambda \approx 1.1 - 1.2$. Thus, in Figure 3.13 the result of this parameter fitting can be seen, giving a value of $\mu_{ela} = 16.5kPa$.

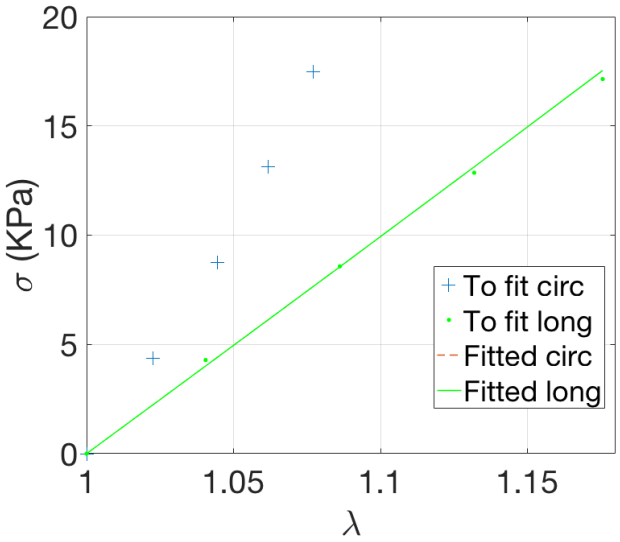

Figure 3.13: Graphical representation of the obtain of the term μ. It only fits for the longitudinal direction since we have seen than collagen is almost concentrated in the circumferential direction.

With the contribution of collagen defined previously, the overall tissue can be characterized. The parameters to fit are B_{col} and N_{col}, both referred to collagen, because the parameter of elastin is defined as its behavior has been assumed to be Neo-Hookean. The functional to be optimized is the same expressed in Eq.2.58 but inserting both directions and the isotropic contribution term. Finally, Figure 3.13 has been resulted out of this process giving the values summarized in Table 3.11.

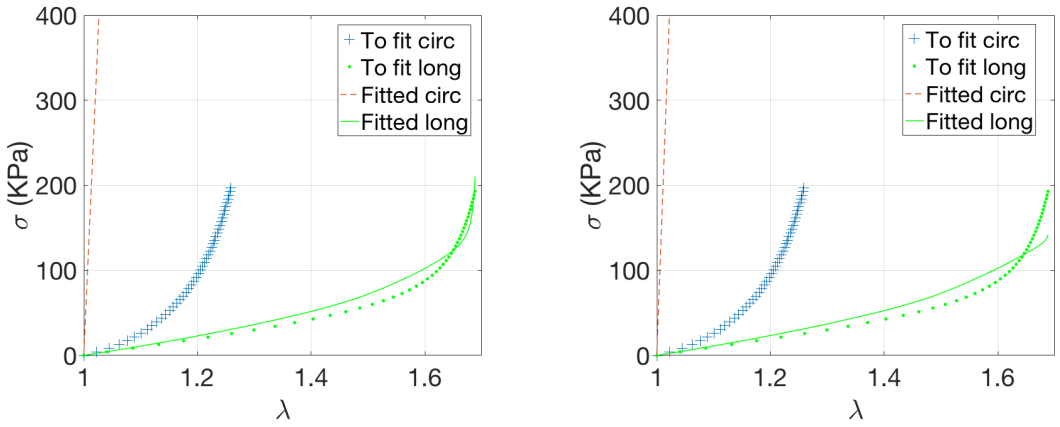

Figure 3.14: Representation of the stress-stretch behavior of a network of collagen and elastin by considering an isotropic Neo-Hookean behavior of elastin – for the WLC (left) and the FJC (right) –

Notice that the generated curve for the circumferential direction did not fit

Table 3.11: Parameters obtained from the fitting process by considering a Neo-Hookean elastin contribution

Collagen fibers	$B_{col}(kPa)$	N_{col}	ϵ_{long}
WLC	317.7876	2.8390	0.1172
FJC	1547.6110	2.8150	0.2297

the experimental data for any of the both models considered. For this reason, the error ϵ is calculated only for the longitudinal direction.

All components into the surface integration

In the second consideration, we assume the elastin contribution to be in the integration over the micro-sphere surface, but with no fiber dispersion acting on their fibers. This condition can be easily summarized as:

$$\tau_f = \left\langle ((\rho\Phi'_{col} + \Phi'_{ela})\lambda_f^{-1}\bar{t} \otimes \bar{t}) \right\rangle \tag{3.4}$$

Then, by summing collagen and elastin contribution sharing the same λ, can be stated that they are working in a disposition in parallel. This assumption was also present in the previous consideration, but in this case might be even accentuated. May be possible that the non-fitting circumferential curve in the previous consideration can be related to this assumption, but this fact will be discussed later on. Moreover, by using the parameters of collagen obtained in Section 3.1.2, the parameters B_{ela} and N_{ela} corresponding to the fibers are going to be fitted now. An analogous process as before shall be done – considering the same orientation vectors Q and the same concentration parameters κ_i – , but the Neo-Hookean contribution of elastin will be neglected. Said that, the values obtained in Tables 3.7 and 3.8 – for two different Specimens of collagen – will be fixed for collagen, while the parameters B_{ela} and N_{ela} are those which are going to be fitted.

Consequently, Table 3.12 recalls the parameters of elastin by fixing the values of real components of collagen. The Figures related are not displayed because they do not fit in any of both stress directions. To overcome this fact, has been tried to follow the same fitting procedure but, instead of fixing the collagen parameters, one has been considered an upper and lower constraint between both Specimens to improve the flexibility of the fitting. Then, Figure 3.15 has been obtained as a result of this procedure. As can be seen, the longitudinal direction fits properly but, again, the circumferential direction that can be attributed almost entirely to the collagen does not adjust to the data. Although the parameters obtained now – See Table 3.13 – seem to be in the same order of magnitude that the previous ones, another approach shall be taken in order to get an accurate adjustment.

Table 3.12: Material parameters of elastin identified by fixing the parameters of collagen with the ones obtained in Section 3.1.2.

Elastin parameters		B_{ela} [kPa]	N_{ela}	ϵ
Specimen A	WLC	0.4987	41.7881	-
	FJC	643.6938	2.9471	-
Specimen B	WLC	0.0049	4.1753	-
	FJC	0.000209	10.9536	-

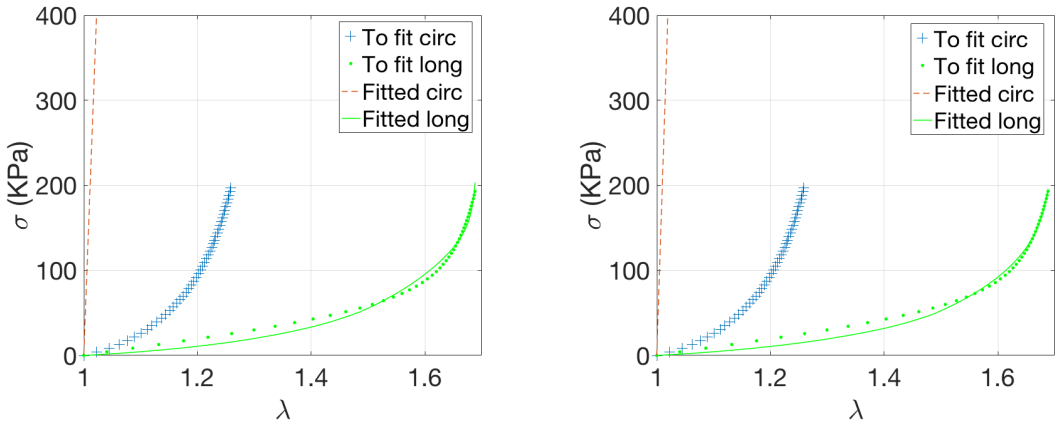

Figure 3.15: Representation of the stress-stretch behavior of a network of collagen and elastin modelled by the micro-sphere based model. For this procedure, the collagen parameters were constrained and the elastin parameters left free – for the WLC (left) and the FJC (right) –.

Table 3.13: Material parameters of elastin identified by constraining the parameters of collagen between a range of those obtained in Section 3.1.2.

Network fibers	$B_{col}(kPa)$	N_{col}	$B_{ela}(kPa)$	N_{ela}	ϵ_{long}
WLC	385.0975	2.8497	10.8117	3.7204	0.0677
FJC	474.9200	2.0390	38.0052	2.9084	0.0579

Finally, as the latter adjustment has not result to fit properly, the same process will be done, but instead of fixing the parameters of collagen with the known values, they are going to be all left free. That is, a four-parameter fitting process is taken into account by estimating B_{col}, N_{col}, B_{ela} and N_{ela}. By this assumption, Figure 3.16 shows that leaving all the parameters free, this experimental data can be fitted. The values obtained are summarized in Table 3.14.

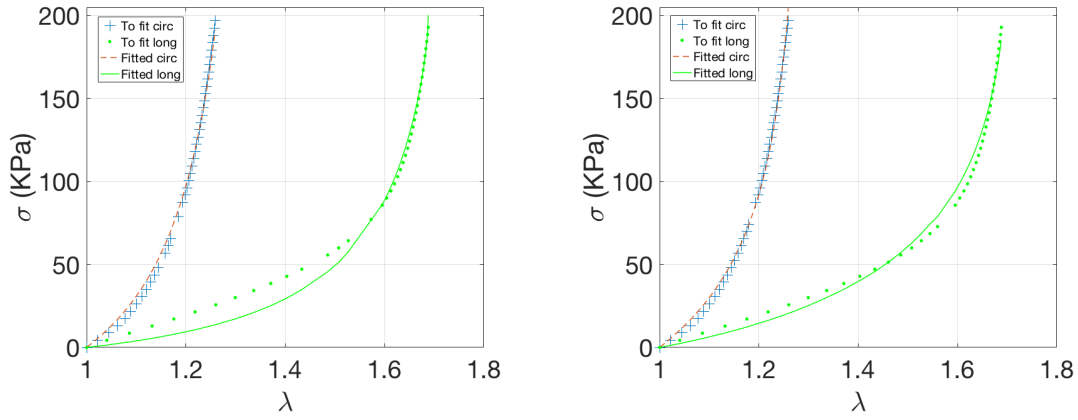

Figure 3.16: Representation of the stress-strech behavior of a network of collagen and elastin modelled by the micro-sphere based model. This procedur considered all parameters left – for the WLC (left) and the FJC (right) –.

Table 3.14: Material parameters of collagen and elastin identified for a four-parameter fitting procedure

Network fibers	$B_{col}(kPa)$	N_{col}	$B_{ela}(kPa)$	N_{ela}	ϵ
WLC	1.6072	1.9968	10.4829	3.2345	0.0545
FJC	5.5739	1.7000	57.7340	2.9504	0.0457

4 Discussion

Along all this work, we have reviewed many relevant aspects of the elasticity of soft tissues – biological tissues mainly –, analyzing their mechanical behavior and trying to summarize into a clear way all the background theory that holds these particular materials. With the aim to understand and explore one of the key challenge of soft materials, how do the micro-scale behavior of soft tissues relate to the macroscopic network mechanical response, representative data from many authors and materials has been progressively reviewed and modeled. We started dealing with single chains or molecules of DNA and collagen, to finally work with networks composed of elastina and collagen.

For what remains to the mechanics of micro-structural components analyzed with single-chain models – the WLC and the FJC –, the application into DNA and collagen at different scales showed several points to be discussed. In the case of DNA, the three variations of the WLC were successfully tested into experimental data and without many remarkable differences to be accounted. Only comment that the reduced version report the smallest error for both Specimens, but for Specimen B, the values of the material parameters present greater differences with the material parameters obtained from the other variations. For these reasons, one decided to use the standard WLC for the following fittings. Furthermore, the FJC was also successfully applied to the DNA but it gave greater fitting errors. Despite of this fact, for the same scheme of two-parameter fitting – for the WLC the parameter to fit were A and L, and for the FJC were L and l –, the FJC was able to get the other material parameters as r_0 and N with the relations $r_0^2 = Nl^2$ and $L = Nl$.

For the single-chain models applied to tropocollagen molecules, the same conclusion than for the DNA can be extracted. Although the WLC gave a smaller error for the fitting, the FJC was able to obtain all the characteristic material parameters of the tropocollagen molecules. Otherwise, an important discrepancy has been found for collagen fibrils. Although collagen fibrils can be understood as a micro-scale of collagen, a macroscopic treatment by using classical network models – 8CH-WLC and 8CH-FJC – was used to overcome the discrepancies that resulted from the single-chain models.

In the macroscopic scale, rubber materials and the cardiovascular tissue have been analyzed. As opposed to the case of collagen fibrils exposed above, for rubber materials, single-chain models has not got much sense. There is the need to use "macroscopic" models such as phenomenological or classical network models. The 8CH-WLC and the 8CH-FJC were also applied to fit the experimental data of Treloar[**?**], obtaining a smaller error for the 8CH-FJC.

Finally, for the cardiovascular tissue, full-network models were applied. The micro-sphere based model was used to link the kinematics of collagen and elastin chains in the micro-scale to the overall macroscopic network. This transition was done by considering the additive split $\Psi = \Psi_{ani} + \Psi_{iso} + \Psi_{vol}$, and this decomposition assumes the fibers to work in a disposition in parallel. This consideration traduces in that the force/stress F_{tot} applied into two chains/fibers in parallel are transmitted into different ways ($F_{tot} = f_1 + f_2$; for $f_1 \neq f_2$) if both chain have different characteristics, but also that the total stretch induced will be the same for both chains/fibers $\lambda_{tot} = \lambda_1 = \lambda_2$.

Moreover, the collagen anisotropy was well reproduced by the Bingham distribution and resulted that collagen fibers were distributed mainly in the circumferential direction. Alternatively, elastin was considered to be distributed along all directions. Thus, the results obtained from the fittings indicate that neither assuming the elastin to have an isotropic neo-hookean response nor considering real collagen material parameters, were able to fit the experimental data. Only by a four-parameter fitting scheme – $B_{col}, N_{col}, B_{ela}, N_{ela}$ – an accurate fitting of the experimental data was obtained – the error of the fitting has been smaller for the FJC than for the WLC. –. The fact that considering *real* parameters obtained from a fibril of collagen/elastin does not work properly, but the model is able to give a solution with a qualitatively small error leaving all the parameters free makes one to think in a possible reason for this. This reason could be the consideration of a disposition in parallel of the fibers. Therefore, a disposition in serie may be an interesting object of study to resolve this discrepancy. By considering two elements to work in serie, their corresponding stretches will not be equal $\lambda_1 \neq \lambda_2$ and also $\lambda_{tot} = \lambda_1 \cdot \lambda_2$ but the force/stress transmitted to each element will be equal to the total force/stress applied to the network $f_1 = f_2 = F_{tot}$. That will imply that, the strain energy functions that we used to derive the stress-stretch relationships, to be recalled in terms of $W = W(f)$ instead of $W = W(\lambda)$. To end with this discussion, an example of two chain acting in parallel and in serie is presented (See Figure 4.1).

Summary of the conclusions and future directions

From all the review done and the results obtained during the work, some conclusions are summarized:

The WLC has given a smaller error of fitting for the micro-scale modeling, while for the macroscopic treatment, the FJC – in cooperation with the 8CH or the micro-sphere based model – exhibited better adjustments than the WLC.

Even a material is considered to be at a micro-scale, a macroscopic treatment

can be required to define its mechanical behavior. In the opposite case, has no sense to apply single-chain models at macro-scales – without considering the micro-sphere based model –.

The application of the full-network models considering a disposition in parallel of their fibers were found to give small errors, but did not work properly by using real parameters obtained from previous adjustments. Then, to assume a disposition in parallel of their fibers will be an interesting alternative to be contemplated.

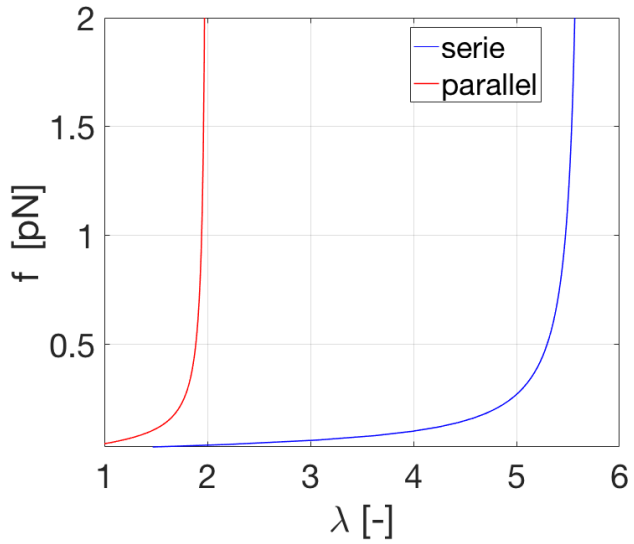

Figure 4.1: Force-stretch relationship for two elements – element 1 and element 2 – in different dispositions. The FJC was used to reproduce the curve with the material parameters $N_1 = 4$, $L_1 = L_2 = 1.4[\mu m]$ and $N_2 = 8$.

Bibliography

[1] Steven B. Smith, Laura Finzi and Carlos Bustamante. Direct Mechanical Measurements of the Elasticity of single DNA Molecules by Using Magnetic Beats.
American Association for the Advancement of Science, Vol.258, No.5085(Nov. 13, 1992) pp. 1122-1126 , November 1992.

[2] A.R. Pasadín, I. Pérez. Fatigue performance of bituminous mixture made with recycled concrete aggregates and waste tire rubber.
Construction and Building materials, 157(2017) 26–33, September 2017.

[3] Kunal Bisht, P.V. Ramana. Evaluation of mechanical and durability properties of crumb rubber concrete.
Construction and Building materials, 155(2017) 811–817, September 2017.

[4] Arun Mohan C M, Sowmya V Krishnankutty. Bridge Bearings - A Review.
International Research Journal of Engineering and Technology (IRJET) , Vol.4, Issue 1, 674–677, January 2017.

[5] http://www.archiexpo.com/prod/mageba/product-126411-1333289.html
Last access 30 of July 2018, 18:24 hours.

[6] http://www.tecnoav.cl/juntas-de-dilatacion-puentes-medianos-a-grandes/
Last access 30 of July 2018, 18:27 hours.

[7] https://www.thinglink.com/scene/494322688282591232
Last access 30 of July 2018, 18:29 hours.

[8] https://en.wikipedia.org/wiki/Entropy
Last access 1 of August 2018, 13:52 hours.

[9] Serdar Göktepe. Micro-macro approaches to rubbery and glassy polymers: Predictive micromechanically-based models and simulations.
Thesis October 2017.

[10] Boris Mergell and Ralf Everaers Tube Models for Rubber-Elastic Systems *Macromolecules*,2001, 34, 5675-5686 December 2000.

[11] Kheng Lim Goh, Anne Listrat, and Daniel Béchet. Hierarchical Mechanics of Connective Tissues: Integrating Insights from Nano to Macroscopic Studies. *Journal of Biomedical Nanotechnology*, Vol.10, 2464-2507, 2014 March 2014.

[12] Archilleas D. Teocharis, Spyros S. Skandalis, Chrysostomi Gialeli, Nikos K. Karamanos. Extracellular matrix structure.
Advanced Drug Delivery Reviews, 97(2016), 4–27 November 2015.

[13] L. Debelle, A.M. Tamburro. Elastin: molecular description and function.
The International Journal of Biochemistry and Cell Biology, 31(1999), 261–272 August 1998.

[14] Lanti Yang. Mechanical Properties of Collagen Fibrils and Elastic Fibers Explored by AFM.
Thesis February 2008.

[15] Baptiste Depalle, Zhao Qin, Sandra J. Shefelbine, Markus J. Buehler. Influence of cross-link structure, density and mechanical properties in the mesoscale deformation mechanisms of collagen fibrils.
Journal of the Mechanical Behavior of Biomedical Materials, 52(2015), 1–13 July 2014.

[16] Marc T. Galloway,MD Andrea L. Lalley, BS Jason T. Shearn, PhD. The Role of Mechanical Loading in Tendon Development, Maintenance, Injury and Repair.
The Journal of Bone and Joint Surgery, 95(2017) : 1620, September 2013.

[17] Daniel T.N. Chen, Qui Wen, Paul A. Janmey, John C. Crocker and Arjun G. Yodh. Rheology of soft materials.
The Annual Review of Condensed Matter Physics, 2010. 1:301-22, May 2010.

[18] Ellen Kuhl, Krishna Garikipati, Ellen M. Arruda, Karl Grosh.
Remodeling of biological tissue: Mechanically induced reorientation of a transversely isotropic chain network. *Journal of the Mechanics and Physics of Solids*, 53(2005) 1552–1573, March 2005.

[19] $https://userpages.uni-koblenz.de/\ rathgeber/Lectures/Chap3_{C}hain_{M}odels.pdf$
Last access 26 of September 2018, 11:49 hours.

[20] L.R.G. Treloar
The elasticity and related properties of rubbers. *Rep. Prog. Phys. 1973 36 755-826*, 1972 36 755-826, August 1972.

[21] Ray W. Ogden, Giuseppe Saccomandi and Ivonne Sgura.

On Worm-like Chain Models within the Three-Dimensional Continuum Mechanics Framework. *Mathematical, Physical and Engineering Sciences*, Vol.462, No.2067(March 8, 2006), pp.749–768 March 2006.

[22] Mary C. Boyce and Ellen M. Arruda.
Constitutive Models of Rubber Elasticity: A Review. *Rubber Chemistry and Technology* July 2000.

[23] Radoslaw Jedynak.
Approximation of the inverse Langevin function revisited. *Rheologica Acta*, Vol.54, Issue 1, 29–39 January 2015.

[24] Sunny Jigger Mistry.
A Micro-Mechanically Based Continuum Model for Strain-Induced Crystallization in Natural Rubber. *A dissertation submitted in partial satisfaction of the requirements for the degree of Doctor of Philosofy in Engineering-Mechanical Engineering.* Spring 2014

[25] C. Miehe, S. Göktepe, J. Méndez Diez.
Finite viscoplasticity of amorphous glassy polymers in the logarithmic strain space . *International Journal of Solids and Structures*, 46(2009) 181–202 August 2008

[26] V. Alastrué, M.A. Martínez, M. Doblaré, A. Menzel.
Anisotropic micro-sphere based finite elasticity applied to blood vessel modelling . *Journal of the Mechanics and Physiscs of Solids*, 57(2009) 178–203 September 2008

[27] V. Alastrué, P. Sáez,M.A. Martínez, M. Doblaré .
On the use of the Bingham statistical distribution in microsphere-based constitutive models for arterial tissue. *Mechanics Research Communications*, 37(2010) 700–706 October 2010

[28] Steven B. Smith, Laura Finzi and Carlos Bustamante.
Direct Mechanical Measurements of the Elasticity of Single DNA Molecules by Using Magnetic Beads. *American Association for the Advancement of Science*, Vol.258, No.5085(1992) 1122–1126 November 1992

[29] Markus J. Buehler and Sophie Y. Wong.
Entropic Elasticity Controls Nanomechanics of Single Tropocollagen Molecules. *Biophysical Journal*, Vol.93, 37–43 July 2007

[30] S.J. Eppell, B.N. Smith, H. Kahn and R. Ballarini.
Nano measurements with micro-devices: mechanical properties of hydrated collagen fibrils. *Journal of The Royal Society Interface*, 3(2006) 117–121 July 2011

[31] Shaofan Li, Bohua Sun.
Advances in Soft Matter Mechanics. *Springer Science and Business Media*, 2012, 9–11 April 2012

[32] John F. Marko, Eric D. Siggia.
Stretching DNA. *Macromolecules*, 1995, 28, 8759–8770 May 1995

[33] Yunjie Wang, Shahrokh Zeinali-Davarani, Yanhang Zhang.
Arterial mechanics considering the structural and mechanical contributions of ECM constituents. *Journal of Biomechanics*, 49(2016) 2358–2365 February 2016

[34] Cristopher Bingham.
An antipodally simetric distribution on the sphere. *The Annals of Statistics*, 1974, Vol.2, No.6, 1201–1225 January 1974

[35] Laurent Bozec and Michael Horton.
Topography and Mechanical Properties of Single Molecules of Type I Collagen Using Atomic Force Microscopy. *Biophysical Journal*, 2005, Vol.88, No.6, 4223–4231 June 2005

[36] P. Saez, A. García, E. Pe na, T. C. Gasser, and M. A. Martínez Microstructural quantification of collagen fiber orientations and its integration in constitutive modeling of the porcine carotid artery. *Acta Biomat.*,2016, 33:189–93 March 2005